Remote Sensing of Environment 167 (2015) 229–246

Contents lists available at ScienceDirect

Remote Sensing of Environment

journal homepage: www.elsevier.com/locate/rse

Spectral and spatial requirements of remote measurements of pelagic *Sargassum* macroalgae

Chuanmin Hu [a,*], Lian Feng [a], Robert F. Hardy [a,b], Eric J. Hochberg [c]

[a] College of Marine Science, University of South Florida, 140 Seventh Avenue South, St. Petersburg, FL 33701, USA
[b] Florida Fish and Wildlife Conservation Commission, Fish and Wildlife Research Institute, 100 Eighth Avenue SE, St. Petersburg, FL 33701, USA
[c] Bermuda Institute of Ocean Sciences, 17 Biological Station, Ferry Reach, St. George's GE01, Bermuda

ARTICLE INFO

Article history:
Received 14 June 2014
Received in revised form 15 May 2015
Accepted 20 May 2015
Available online 14 June 2015

Keywords:
Sargassum
Macroalgae
Remote sensing
MODIS
Landsat
MERIS
WorldView-2
AVIRIS
HICO
HyspIRI
GEO-CAPE

ABSTRACT

Remote detection of pelagic *Sargassum* is often hindered by its spectral similarity to other floating materials and by the inadequate spatial resolution. Using measurements from multi-spectral satellite sensors (Moderate Resolution Imaging Spectroradiometer or MODIS), Landsat, WorldView-2 (or WV-2) as well as hyperspectral sensors (Hyperspectral Imager for the Coastal Ocean or HICO, Airborne Visible-InfraRed Imaging Spectrometer or AVIRIS) and airborne digital photos, we analyze and compare their ability (in terms of spectral and spatial resolutions) to detect *Sargassum* and to differentiate it from other floating materials such as *Trichodesmium*, *Syringodium*, *Ulva*, garbage, and emulsified oil. Field measurements suggest that *Sargassum* has a distinctive reflectance curvature of ~630 nm due to its chlorophyll c pigments, which provides a unique spectral signature when combined with the reflectance ratio between brown (~650 nm) and green (~555 nm) wavelengths. For a 10-nm resolution sensor on the hyperspectral HyspIRI mission currently being planned by NASA, a stepwise rule to examine several indexes established from 6 bands (centered at 555, 605, 625, 645, 685, 755 nm) is shown to be effective to unambiguously differentiate *Sargassum* from all other floating materials Numerical simulations using spectral endmembers and noise in the satellite-derived reflectance suggest that spectral discrimination is degraded when a pixel is mixed between *Sargassum* and water. A minimum of 20–30% *Sargassum* coverage within a pixel is required to retain such ability, while the partial coverage can be as low as 1–2% when detecting floating materials without spectral discrimination. With its expected signal-to-noise ratios (SNRs ~ 200:1), the hyperspectral HyspIRI mission may provide a compromise between spatial resolution and spatial coverage to improve our capacity to detect, discriminate, and quantify *Sargassum*.

1. Introduction

Sargassum spp. is a brown macroalga that is abundant in the Gulf of Mexico (GOM) and the Atlantic (Gower & King, 2011; Gower, Hu, Borstad, & King, 2006). Providing food, shade, and shelter to fish, shrimp, crabs, turtles, and other marine organisms (Council, 2002; Rooker, Turner, & Holt, 2006; Witherington, Hirama, & Hardy, 2012), *Sargassum* serves as an important habitat in the marine ecosystem. *Sargassum* may also play an important role in marine primary productivity (Gower et al., 2006), nutrient remineralization, dynamics of colored dissolved organic matter, and bacterial activities (Lapointe, 1995; Lapointe, West, Sutton, & Hu, 2014; Zepp, Shank, Vähätalo, Bartels, & Jones, 2008). In coastal zones, *Sargassum* can be a natural fertilizer for dune plants, helping prevent coastal erosion (Anthony, Vanhee, & Ruz, 2006; Tsoar, 2005). On the other hand, excessive *Sargassum* on the beach is a burden to local coastal managers as they represent a nuisance and a health hazard, and thus must be physically removed. For example, in Texas of the United States, local management agencies needed to rent equipment to remove *Sargassum* from the beaches almost every year. Indeed, many beaches around the GOM and the southern Caribbean are subject to *Sargassum* deposition on a regular basis (Gower, Young, & King, 2013).

Accurate knowledge of *Sargassum* distributions and their temporal changes helps quantify their role in modulating local biogeochemistry and carbon cycling. Timely information on the occurrence of *Sargassum* is useful for both research and management such as implementation of harvesting policy, equipment rental for beach cleaning, and providing guidance on planning field surveys and recreational fishing. When such information is not available in near real-time, retrospective analysis of *Sargassum* distributions can also help understand local ecology and physical processes (e.g., eddies and eddy fronts). To date, remote sensing has served as the primary means to study *Sargassum* distributions. Unfortunately, due to technical limitations, detecting *Sargassum* or quantifying *Sargassum* biomass has been difficult, not to mention performing these tasks in near real-time.

Gower et al. (2006) is perhaps the first study that demonstrates the use of the Medium Resolution Imaging Spectrometer (MERIS) satellite

* Corresponding author.
E-mail address: huc@usf.edu (C. Hu).

http://dx.doi.org/10.1016/j.rse.2015.05.022
0034-4257/

instrument to detect *Sargassum* in the GOM. Since then, several recent studies showed the capacity of other satellite sensors (e.g., Moderate Resolution Imaging Spectroradiometer or MODIS, Landsat TM and ETM+, Geostationary Ocean Color Imager or GOCI) in detecting *Sargassum* or other floating macroalgae (Hu, 2009; Hu, Cannizzaro, Carder, Muller-Karger, & Hardy, 2010a; Son, Min, & Ryu, 2012). MERIS was also used to derive time-series of *Sargassum* distributions in the GOM and North Atlantic (Gower & King, 2011; Gower et al., 2013). These studies are based on the principle that *Sargassum* macroalgae are floating vegetation on the sea surface and therefore would cause enhanced reflectance in the near-infrared or NIR (the red-edge effect, i.e., enhanced reflectance between 700 and 730 nm). For example, Gower et al. (2006) used the MERIS Maximum Chlorophyll Index (MCI (Gower, King, Borstad, & Brown, 2005)) to examine the radiance signal at 709 nm relative to the neighboring wavelengths, and Hu (2009) used the Floating Algae Index (FAI) to examine the MODIS reflectance signal at 859 nm relative to the two neighboring bands at 645 and 1240 nm. *Sargassum* macroalgae cause increased MCI and FAI values as compared with *Sargassum*-free waters, thus making delineation of these features straightforward. The advantage of FAI is that the concept can be extended to Landsat TM and ETM+ as well as to the most recent Operational Land Imager (OLI) onboard Landsat 8 (February 2013–present), leading to a Landsat FAI which can be used to detect small features, as all these Landsat sensors have much higher spatial resolution (30 m) than MODIS (250 m) and MERIS (300 m). Furthermore, FAI is less sensitive than other popular indexes (e.g., Normalized Difference Vegetation Index or NDVI) to changes in atmospheric conditions or solar/viewing geometry, thus making it easier to compare images.

Based on the red-edge concept, time-series of *Sargassum* distributions in the GOM and Atlantic have been documented by Gower and King (2011); and Gower et al. (2013) through analysis of MERIS data, and near real-time FAI imagery for the GOM and central Atlantic have been generated and updated daily at the University of South Florida ((Hu, Barnes, Murch, & Carlson, 2014); http://optics.marine.usf.edu, under "Satellite Data Products" and "C Atlantic", Fig. 1). These near real-time FAI products have been used routinely by local environmental groups to monitor potential *Sargassum* landing along the beaches of Texas (Prof. Thomas Linton, University of Texas at Galveston, personal comm.) and the Lesser Antilles Islands (Dr. Jean-Philippe Maréchal, Caribbean Global Coral Reef Monitoring Network (GCRMN) advisor). However, at least two limitations exist in these previous analyses and near real-time data products.

First, *Sargassum* is not the *only* marine organism that causes elevated red-edge reflectance. Other organisms or materials floating on the surface, such as *Trichodesmium* and floating seagrass *Syringodium* can all cause red-edge reflectance. Other floating materials such as marine debris or garbage or emulsified oil (e.g., during the Deepwater Horizon (DWH) oil spill in the GOM between April and July 2010, or from other oil platforms) can lead to enhanced reflectance in all NIR wavelengths, but not cause red-edge reflectance. Fig. 2 shows the typical reflectance spectra from these materials, including the green macroalgae *Ulva prolifera* found in the Yellow Sea and East China Sea (Hu et al., 2010b) (the methods to collect these spectra are detailed in the section below). All these different floating materials show enhanced NIR reflectance. Unless some *a priori* knowledge is available, it is currently difficult to tell whether a delineated ocean feature is *Sargassum* or something else. Hu, Cannizzaro, Carder, Muller-Karger, and Hardy (2010a)

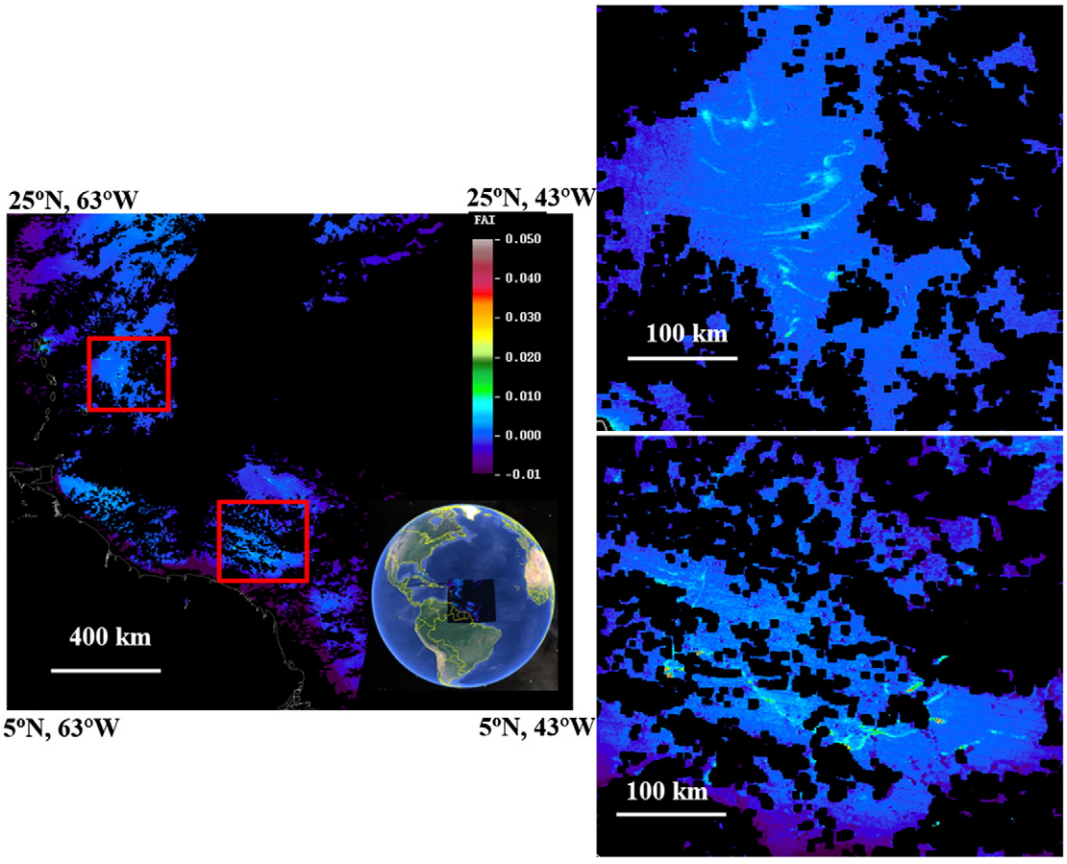

Fig. 1. MODIS/Terra FAI image on 1 July 2012 (14:15 GMT) over the central West Atlantic showing surface slicks with enhanced NIR reflectance. Black color indicates land or clouds or sun glint mask. Although the spectral shapes of the large slicks do not appear similar to those of *Trichodesmium* (Hu et al., 2010b), due to lack of spectral resolution it is hard to conclude with 100% certainty that they are *Sargassum* macroalgae.

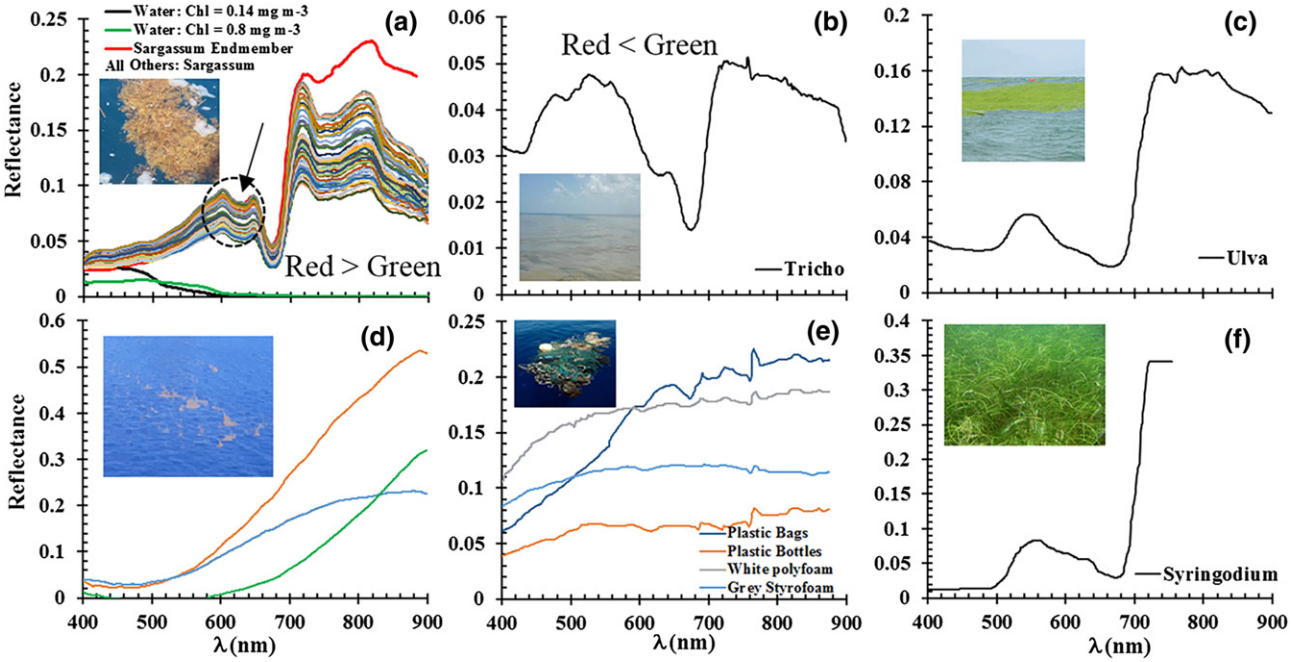

Fig. 2. (a) Surface reflectance spectra (*R*, dimensionless) of *Sargassum* mats and nearby waters measured in the GOM and off Bermuda. Note the local reflectance minimum around 632 nm (black arrow) due to the chlorophyll c pigment absorption, and the enhanced reflectance between 580 and 650 nm (dotted circle) as compared with the reflectance below 550 nm. Reflectance plotted in red was measured from field collected *Sargassum* aggregated in a bucket on the ship deck, thus representing pure *Sargassum* endmember. (b)–(f) Surface reflectance spectra for *Trichodesmium*, *Ulva prolifera*, emulsified oil, various garbage materials, and seagrass *Syringodium*. See text for more details on how these spectra were collected. For illustrative purpose, reprehensive photographs are inset in each panel. The oil spectra were collected by AVIRIS with spectral signature around 1.2 and 1.7 μm (Clark et al., 2010).

combined MODIS land and ocean bands to examine the spectral shape in the blue and green wavelengths to diagnose whether an FAI-based feature is due to *Trichodesmium*. This is because *Trichodesmium* has several spectral signatures in the blue and green, making such "fingerprinting" possible. However, such finger printing of *Trichodesmium* is possible only for some special cases where the floating materials occupy a large or full portion of a satellite image pixel (see sensitivity analysis below), and such a requirement can often not be met by MODIS due to the 500-m and 1000-m resolution data used to examine the spectral shape. Nevertheless, it is well understood that if a certain organism or material has unique spectral shapes, spectral finger printing is possible. *Sargassum* also has some unique spectral features between 600 and 650 nm due to its chlorophyll c pigments (see below), yet none of the multi-band ocean color sensors are equipped with several spectral bands in this spectral range, making spectral discrimination difficult.

Second, *Sargassum* patches can be very small, on the order of several m^2 or even smaller. Even the Landsat sensors at 30-m ground resolution may not be able to detect the small *Sargassum* patches. For example, using 0.4-m resolution data collected by an airborne Portable Hyperspectral Imager for Low-Light Spectroscopy (PHILLS) from southwest Florida, Szekielda, Marmorino, Bowles, and Gillis (2010) reported that only 2.3% of the ocean area was found to contain *Sargassum*, with only 0.2% of the pixels containing full *Sargassum* coverage. Although this is a case study for a limited area from which it is impossible to generalize for the entire GOM or the Atlantic, the case study as well as the analysis below does show that small *Sargassum* patches are abundant, and they may not be detected by coarse-resolution sensors. For the same reason, some or all delineated features may be a mixture of floating materials and water, and an unmixing scheme may be required to accurately estimate the *Sargassum* coverage (area) or biomass.

During the DWH oil spill, a variety of remote sensing techniques were used to assess the spill coverage and quantity (Clark et al., 2010; Garcia-Pineda et al., 2013; Hu et al., 2011). These include the airborne digital photographs and Airborne Visible-InfraRed Imaging Spectrometer (AVIRIS) measurements. Depending on the flight altitude, they usually have ground resolution of centimeters and meters, respectively. In addition, the hyperspectral data collected by the Hyperspectral Imager for the Coastal Ocean (HICO (Lucke et al., 2011)) sensor on the International Space Station (ISS) have been released, making it possible to diagnose the spectral shape of the delineated features. However, these measurements are irregular and their coverage is scarce; thus, they can only be used for event response (in the case of AVIRIS) and demonstration of concepts (in the case of HICO). Routine assessment of the coastal water environments using these hyperspectral measurements is not possible.

The situation may be changed with a new mission currently being planned by NASA. The mission is targeted to global ecosystems with a particular emphasis on coastal zones, namely the Hyperspectral Infrared Imager (HyspIRI) mission (Devred et al., 2013). HyspIRI was originally expected to be a hyperspectral sensor covering 380–2500 nm (10 nm increments) with a ground resolution of 60 m, a swath width of 145 km, and an equatorial revisit frequency of every 19 days (Devred et al., 2013) (Table 1). In 2014, a review conducted by NASA's Jet Propulsion Lab (JPL) in order to see how to support Sustainable Land Imaging (SLI) for the next twenty-five years (a congressional mandate) proposed new technology that would enable a Visible-Shortwave Infrared (VSWIR) spectrometer with 30-m resolution, 185-km swath width, and a 16-day revisit (Dr. Robert Green, JPL, personal comm.). Unlike other precursors such as the Hyperion sensor on the EO-1 mission, HyspIRI will be customized for its spatial and spectral resolutions as well as its coverage and radiometric sensitivity, providing global data with a particular focus on coastal zones. In this study, HyspIRI is assumed to have the originally designed 60-m resolution.

Thus, given the availability of the multi-sensor data at various ground resolutions and spectral resolutions and given the need to design and implement the HyspIRI mission, the objective of this study is to provide recommendations on spectral and spatial requirements of future hyperspectral satellite missions (including HyspIRI) in order to

Table 1
Space- and airborne data that were used in this study. These include data collected by MODIS, Landsat, HICO, AVIRIS, WorldView-2, and airborne digital photos. The specifications of the HyspIRI mission are also provided in the last two rows.
Original specifications provided in Devred et al. (2013).

Sensor	Spatial resolution	Swath	Spectral range	Spectral resolution	Revisit
MODIS	250–1000 m	2330 km	412–2130 nm	Multi-band	Near daily
Landsat	30 m	180 km	450–1640 nm	Multi-band	16 days
HICO	90 m	45 km	350–1000 nm	5.7 nm	Irregular
AVIRIS	8–15 m	20–40 km	350–2500 nm	10 nm	Event response
WV-2	2 m	~17 km	400–1040 nm	Multiband	Irregular
Photologger	cm	<1 km	RGB photo	N/A	Event response
HyspIRI*	60 m	145 km	380–2500 nm	10 nm	19 days
HyspIRI[a]	30 m	185 km	380–2500 nm	10 nm	16 days

[a] New specifications proposed more recently (Dr. Robert Green, JPL, personal comm.) Note that in this study the spatial resolution is assumed to be 60 m.

effectively detect and quantify *Sargassum*, with the following two questions to be addressed:

1) What are the optimal band centers and bandwidths required for such a task?
2) What is the spatial detection limit once these spectral requirements are met? In other words what is the minimal *Sargassum* portion of an image pixel that can be detected and spectrally differentiated?

The questions are addressed using two approaches. One is through simulations using existing endmember spectra and realistic noise from satellite-derived reflectance data, and the other is through comparison of measurements by several different sensors in their capacity to detect and quantify *Sargassum*, with specific focus on the spectral and spatial resolutions. Although the focus is on *Sargassum*, these approaches are also applicable to other floating materials.

The paper is organized as follows. The methods to collect and process field, airborne, and satellite data are described first, followed by the methods to perform the spectral analysis and spatial simulations. Then, several image examples together with sample spectra are inspected to demonstrate the possibility of using spectral shapes to differentiate *Sargassum* from other floating materials and the importance of spatial resolutions. These demonstrations are then reinforced by the results from the quantitative spectral analysis to show the spectral requirements, and then followed by the spatial simulations to understand the sensitivity of different sensors and atmospheric correction schemes on the *Sargassum* detection limit. The concept of unmixing is also illustrated using WV-2 data and a linear unmixing model. Finally, the implications of this study to data interpretation and future sensor and algorithm design are discussed.

2. Data and method

2.1. Field data

The endmember reflectance spectra from a variety of floating algae and materials were collected by different groups at different locations following similar protocols. These include *Sargassum* in the GOM and Atlantic (Fig. 2a), *Trichodesmium* in the Florida Keys (Fig. 2b), *U. prolifera* in the Yellow Sea off Qingdao (China) (Fig. 2c), various garbage materials from a field experiment in Tampa Bay (USA) (Fig. 2e), and seagrass *Syringodium* in the Florida Keys (Fig. 2f). Reflectance spectra from emulsified oil were not measured in the field but collected by AVIRIS on 17 May 2010 during the DWH oil spill in the northern GOM (Fig. 2d).

For the *Sargassum* endmember (Fig. 2a), *in situ* data of surface reflectance of both *Sargassum* mats and nearby waters were taken from opportunistic cruises. In September 2011, a cruise survey to the NE GOM was sponsored by the U.S. NOAA, where reflectance was measured using a hand-held above-water spectrometer (Spectrix) following the NASA Ocean Optics protocols (repeated measurements of water, sky, and a reference plaque) (Mueller et al., 2003). In order to collect the pure *Sargassum* endmember spectra, *Sargassum* was collected from the water and carefully put in a bucket full of water on the ship's deck. The reflectance of *Sargassum* was then measured with the Spectrix. On 23 January 2012, a 10 × 10 m *Sargassum* raft was encountered during a coral reef survey off Bermuda using a small boat. A USB2000 (Ocean Optics Inc.) spectrometer was used to measure the *Sargassum* and water reflectance against measurements of a standard Spectralon reflectance plaque (Labsphere, Inc.). Measurements of *Sargassum* and water were at a distance of ~1 m, and a total view area of ~0.1 m^2. About 50 spectra each for *Sargassum* and water were collected. Of all these *Sargassum* spectra, the one collected from the GOM showed the highest NIR reflectance, and therefore was chosen as the endmember for the spectral analysis and spatial simulations. In such simulations, the water endmember spectra were collected during a NEGOM cruise in May 1999 (NEGOM5, see (Hu et al., 2003)) using the same protocols above, with two spectra used to represent typical clear and turbid waters in the GOM: one for chlorophyll a concentration (Chla) of 0.14 mg m^{-3} (NEGOM5 line 11 station 18) and the other for Chla of 0.80 mg m^{-3} (NEGOM5 line 01 station 07). Their corresponding absorption coefficients of colored dissolved organic matter (CDOM) at 443 nm were determined to be 0.012 and 0.050 m^{-1}, respectively.

For the *Trichodesmium* endmember (Fig. 2b), surface reflectance spectra were measured above a *Trichodesmium* patch floating on the water surface in the Florida Keys (24.63°N, 81.08°W) on 1 July 1999 using a hand-held spectrometer (Spectrix) following the same protocols as above. The spectrum shown in Fig. 2b was also used by Hu, Cannizzaro, Carder, Muller-Karger, and Hardy (2010a) to compare with MODIS-derived reflectance spectra.

For the *Ulva* endmember (Fig. 2c), surface reflectance spectra were collected from a bloom patch floating on the water surface off Qingdao in summer 2008 using a hand-held spectrometer following the same protocols as above (He, Liu, Yu, Li, & Hu, 2011).

For the emulsified oil endmember (Fig. 2d), a description of the AVIRIS data collection and processing is provided in the next section.

For the garbage endmember (Fig. 2e), a field experiment was conducted in Tampa Bay during spring 2011 to measure the reflectance spectra of various materials. These materials included gray plastic trash bags, plastic water bottles, white polyfoam, and gray Styrofoam. These materials are often found in marine garbage patches. During the experiment, each type of material (with sufficient size to fill the field-of-view of a hand-held spectrometer) was put in water, and collected after their reflectance spectra were measured. In the simulations, these spectra were averaged to represent a "mean" spectrum for the garbage endmember.

For the *Syringodium* (seagrass) endmember, the spectrum was taken from Dierssen, Chlus, and Russell (2015), who measured the reflectance of floating seagrass in the Florida Keys.

2.2. Airborne and satellite data

Table 1 provides a list of the space and airborne data that were used in this study. These include data collected by MODIS, Landsat, HICO, AVIRIS, WV-2, and airborne digital photographs. The proposed

specifications of HyspIRI are also listed in Table 1. Because of their different characteristics, they were processed differently.

AVIRIS data were obtained from the NASA JPL. During the DWH oil spill, data from a total of 456 flight lines were collected between 6 May and 22 July 2010. The data were provided by JPL as geo-referenced and calibrated radiance. Signal-to-noise ratios (SNRs) between 0.6 μm and 1.7 μm of AVIRIS measurements are typically in a range of 60:1–100:1 (Gao, 1993). Atmospheric correction using the Tafkaa software (Gao, Montes, Ahmad, & Davis, 2000) was first attempted to remove the atmospheric effects and derive the surface reflectance. However, the resulting reflectance spectra often showed negative values in the blue and green wavelengths for unknown reasons. Therefore, total radiance (L_t) was used to examine the spectral shapes of the visually identified features. One exception was the AVIRIS data on 17 May, 2010, which was processed by the USGS to obtain surface reflectance (data courtesy of Dr. Gregg Swayze, USGS).

Airborne photos were collected during the DWH oil spill as part of an effort to locate surface features including oil and *Sargassum*. These photos were taken when certain features were identified by the observer, thus representing subjective sampling in the NE GOM. However, the low altitude and high resolution (estimated to be in the order of centimeters) make them suitable to serve as ground reference data to compare with the observations from other coarse resolution sensors. After the DWH oil spill, an NSF-funded project supported objective airborne mapping of *Sargassum* (Powers, Hernandez, Condon, Drymon, & Free, 2013). These photos were available at and obtained from NOAA. The data archive was searched to find concurrent (same day) and co-located airborne and AVIRIS data. Due to the sparse nature of both types of measurements, only 3 days (18 and 24 May 2010, 12 July 2010) revealed concurrent AVIRIS and airborne photo measurements. Of these 3 days, only 5 of the 24 photos taken on 24 May 2010 showed *Sargassum* mats through visual inspection.

MODIS and HICO data were obtained from NASA Goddard Space Flight Center. The calibrated radiance ($L_t(\lambda)$, where λ is the wavelength) was first corrected for the two-way ozone absorption effect using ozone data collected by the Total Ozone Mapping Spectrometer onboard the Earth Probe spacecraft (or EPTOMS) or TIROS Operational Vertical Sounder (or TOVS), and then converted to the total reflectance as $R_t(\lambda) = \pi L_t(\lambda)/(F_o(\lambda)\cos(\theta_o))$, where $F_o(\lambda)$ is the solar constant adjusted for Earth–Sun distance, and θ_o is the solar zenith angle. Then, contribution from Rayleigh or molecular scattering ($R_r(\lambda)$) was removed from the total reflectance, resulting in the Rayleigh-corrected reflectance:

$$R_{rc}(\lambda) = R_t(\lambda) - R_r(\lambda). \quad (1)$$

Note that compared with the remote sensing reflectance ($R_{rs}(\lambda)$, sr^{-1}) or surface reflectance ($R(\lambda)$, dimensionless) after a full atmospheric correction, $R_{rc}(\lambda)$ is dimensionless and still contains the effects of aerosol scattering, aerosol–Rayleigh interactions, and the two-way transmittance from the sun to the target and from the target to the sensor. Thus, $R_{rc}(\lambda)$ is a result of partial atmospheric correction. The reason to have a partial atmospheric correction is because it is difficult to perform a full atmospheric correction over surface floating features, as the enhanced reflectance in the NIR and SWIR will violate the black-pixel assumption for the full atmospheric correction (Gordon, 1997). The resulting spectral R_{rc} data were map projected to an equidistant cylindrical (i.e., rectangular) projection for further analysis.

Landsat TM and ETM+ data were obtained from the U.S. Geological Survey. The entire data archive was searched for the AVIRIS flight dates in order to compare with AVIRIS observations. Due to the 16-day repeat cycle and frequent cloud cover, concurrent (same day) and collocated Landsat and AVIRIS data were available only on 24 May 2010. Landsat R_{rc} data were derived in the same way as with MODIS and HICO. Note that although Landsat-8 OLI data are also available from the USGS, the data collection did not start until February 2013, and thus OLI data were not used in this study.

WorldView-2 (WV-2) data were obtained from the DigitalGlobe, Inc. (DigitalGlobal Catalog ID 1030010003418B00), acquired on 8 December 2009 at 15:08 GMT. WV-2 data have 8 spectral bands from 400 to 1040 nm at 2-m ground resolution. Bands 7 (770–895 nm), 5 (630–690 nm), and 3 (510–580 nm) were used to compose a red-green-blue (RGB) image for visual inspection of suspect features. The image was projected in UTM Zone 20 North. The projected across-track scan distance is ~16.7 km. The total projected area of the image is ~471.7 km^2.

2.3. Visual inspection and comparison

There is currently no algorithm that can be used to differentiate the various features automatically. The spectral shapes of suspect features identified from the various types of imagery were therefore visually examined. These features were identified visually from the true-color red-green-blue imagery and/or the FAI imagery, with their spectra extracted using a software written in-house. For cross-sensor comparison, the images collected by different sensors were co-registered in the software ENVI or Erdas Imagine, and then visually analyzed.

The concurrent Landsat and AVIRIS, and the concurrent AVIRIS and airborne photos were also visualized to determine qualitatively how different resolutions may affect *Sargassum* detection and quantification.

In addition to the above qualitative analysis and demonstration, quantitative analysis using several indexes and numerical simulations are used to understand the spectral requirements and spatial detection limit in different situations. These methods are described below.

2.4. Definition of indexes

Several indexes were used in this study to differentiate various endmembers. Most of these were developed and used earlier for bloom detection, but two were defined in this study.

The first index is the FAI (Hu, 2009), developed to detect the red-edge reflectance from both MODIS and Landsat. Because the field data (Fig. 2) did not cover the spectral range in the SWIR where one band is required to calculate FAI, FAI data products were generated from MODIS and Landsat only, following the procedures of Hu (2009). FAI is calculated using NIR reflectance referenced against a baseline formed linearly between the red and SWIR bands. Mathematically, it is expressed as:

$$\mathrm{FAI} = R_{rc,NIR} - R_{rc,red} - (R_{rc,SWIR} - R_{rc,red})(\lambda_{NIR} - \lambda_{red})/(\lambda_{SWIR} - \lambda_{red}), \quad (2)$$

where the subscripts NIR, red, and SWIR represent the spectral bands. For MODIS, $\lambda_{NIR} = 859$ nm, $\lambda_{red} = 645$ nm, $\lambda_{SWIR} = 1240$ nm. For Landsat, $\lambda_{NIR} = 660$ nm, $\lambda_{red} = 825$ nm, $\lambda_{SWIR} = 1650$ nm. HICO is not equipped with a SWIR band, and thus was not used to derive FAI but used for spectral analysis.The second index is the NDVI, defined as

$$\mathrm{NDVI} = (R_{NIR} - R_{red})/(R_{NIR} + R_{red}), \quad (3)$$

where R can be reflectance collected in the field or derived from satellite measurements (e.g., R_{rc}). In the absence of a SWIR band, NDVI can also be used to delineate surface floating materials, but it is more prone to perturbations due to variable aerosols, sun glint, and solar/viewing geometry (Hu, 2009).

The third index is the Maximum Chlorophyll Index (MCI (Gower et al., 2005)), defined as

$$\mathrm{MCI} = R_{rc,709} - R_{rc,681} - (R_{rc,754} - R_{rc,681})(709–681)/(754–681), \quad (4)$$

where the numbers represent wavelength centers (in nm) of MERIS bands. MCI was designed to measure the red-edge reflectance of both water-column chlorophyll and floating vegetation, and has been used extensively to map blooms of both types (Gower et al., 2006; Gower & King, 2011; Gower et al., 2013).

The fourth index is the *Sargassum Index* (SI (Dierssen et al., 2015)), defined as

$$SI = R_{r3}/R_{r2}, \quad (5)$$

where "r3" is the wavelength of a local reflectance peak and "r2" is the wavelength of a local reflectance trough. In Dierssen et al. (2015), r3 and r2 were chosen as 650 and 630 nm, respectively, from field-measured spectra. These wavelengths were optimized in this study through determining band centers and band widths using spectra at different resolutions.

The fifth index is the Line Depth (LD), defined as the wavelength interval between the reflectance local trough and the two neighboring local peaks:

$$LD = R_{r1} + (R_{r3} - R_{r1})(\lambda_{r2} - \lambda_{r1})/(\lambda_{r3} - \lambda_{r1}) - R_{r2}, \quad (6)$$

where "r1" is the local reflectance peak at a wavelength shorter than "r2". This design is similar to FAI, and can be used instead of SI for the same argument when FAI is preferred over NDVI. Basically, a band subtraction is less sensitive to environmental perturbations than a band ratio, because most of these perturbations tend to be spectrally flat (e.g. (Hu, Lee, & Franz, 2012b)). The same line depth approach was also used by Dekker (1993) and Qi, Hu, Duan, Cannizzaro, and Ma (2014) to quantify cyanobacterial blooms because of the local absorption maximum around 625 nm by phycocyanin pigment. Note that for the *Sargassum* endmember spectra in Fig. 2a, LD is positive.

Finally, a sixth index is defined as the red/green band ratio (RGR):

$$RGR = R_{r3}/R_{green}. \quad (7)$$

where "green" is a wavelength near 555 nm. The reason to define this index is to differentiate *Sargassum* from *Trichodesmium* because they have opposite red/green ratios (Fig. 2a & b).

2.5. Spectral analysis to determine band centers and band widths

The wavelengths corresponding to local *Sargassum* reflectance peaks and troughs between 595 and 660 nm (Fig. 2a) were determined through a derivative analysis (Hochberg, Atkinson, & Andréfouët, 2003). The peak wavelengths correspond to 0.0 in the first derivative spectra and local maximum in the second derivative spectra. This analysis was repeated three times for the same data but at the original resolution (1 nm), 5-nm resolution, and 10-nm resolution. The reason to use 10-nm resolution was because HyspIRI is expected to have 10-nm resolution continuous bands. The reason to use 5-nm resolution was because another future satellite mission currently being planned by NASA, namely the Geostationary Coastal and Air Pollution Events (GeoCAPE) mission (Fishman et al., 2012), is expected to have 5-nm resolution continuous bands. The coarser-resolution data were constructed *not* through data binning of the 1-nm data but using a running mean (with either 5- or 10-nm band widths) in order to determine the band centers at these spectral resolutions.

Such determined band centers do not necessarily lead to the highest index values when these bands are used to calculate the various indexes (Eqs. (3) – (7)). For example, because the reflectance trough around 630 nm in the *Sargassum* spectra is not equally spaced between the two local maximum-reflectance wavelengths, the wavelength may be shifted to result in a maximum LD value. To determine the optimal band centers for each index, several iterations were used until a maximum index value was reached. This sometimes resulted in different band centers for different spectral resolutions even for the same index, as shown below.

2.6. Sensitivity analysis for spatial resolution requirements: simulations

Without any data analysis, it is intuitive that the finer the spatial resolution, the smaller the *Sargassum* patch that can be captured. Thus, without knowing the size distribution statistics, it is difficult to determine the "optimal" spatial resolution for *Sargassum* (and all other features) detection. Indeed, this is nearly impossible to know such statistics in the near future due to lack of high-resolution (sub meter) data with sufficiently large coverage. Therefore, an alternative way was used to determine the minimum percentage *Sargassum* coverage (P_{min}) in an image pixel with finite size (e.g., 60×60 m^2). Once P_{min} is determined, the minimal size of a *Sargassum* patch that can be detected by a specific sensor can be easily determined as a product of P_{min} and the sensor's spatial resolution.

P_{min} was calculated by mixing the *Sargassum* and water endmembers at variable proportions (P from 0.0 to 1.0) while adding spectral noise (ΔR):

$$R_{mix} = P \times R_s + (1-P)R_w + \Delta R, \quad (8)$$

where R_s is reflectance of the *Sargassum* (or other floating materials) endmember and R_w is the reflectance of the water endmember. Then, the three indexes (NDVI, LD, RGR) were calculated from each noise-added spectrum. For each spectrum of the *Sargassum*-water mixture, 1000 noise values for each band were added. These simulated noise values were spectrally *independent*, following a Gaussian distribution with a zero mean and the standard deviation (ΔR_{STD}) given by two scenarios.

The first scenario used ΔR_{STD} derived from measurements of the Sea-viewing Wide Field-of-view Sensor (SeaWiFS) over the North Atlantic (Table 3 in Hu, Feng, & Lee (2013), values in the parenthesis for Chla = 0.15 mg m^{-3}). These noise values were assumed typical from satellite ocean color measurements over clear waters. They represent the lower bound from the standard atmospheric correction currently used by NASA (Gordon, 1997), because the noise could be higher for coastal waters (Moore, Campbell, & Feng, 2014). For wavelengths not available on SeaWiFS, linear interpolation was used. The noise values in reflectance units (dimensionless) are listed in the second column of Table 2.

The second scenario used noise values expected from HyspIRI measurements under "typical" measurement conditions. The top-of-atmosphere (TOA) radiance ($L_{t,typical}$) over clear waters measured by any satellite sensors is provided in Table 4 of Hu et al. (2012a) for solar zenith angle (SZA) of 45°. $L_{t,typical}$ was converted $R_{t,typical}$. Then, assuming a signal-to-noise ratio (SNR) of 200:1 for all spectral bands of HyspIRI under typical radiance input over clear waters, ΔR_{STD} was then derived as $R_{t,typical}$/SNR. Such derived ΔR_{STD} is listed in the last column of Table 2. The 200:1 assumption was based on HICO measurements over clear waters (Hu, Feng, et al., 2012a), and it is about three times higher than AVIRIS measurements (Gao, 1993). Note that in this scenario the surface reflectance of all endmember spectra in Fig. 2 were increased by 0.02 for all wavelengths in order to mimic R_{rc} derived from satellite measurements. The addition of 0.02 was to approximate aerosol reflectance corresponding to typical aerosol optical thickness of 0.08 for the North Atlantic. Note that this is a simple approximation,

Table 2
Reflectance noise (ΔR_{STD}) used in the sensitivity simulations for the 10-nm bandwidth bands. See Eq. (7) and text for more information.

Band center (nm)	ΔR_{std} (SeaWiFS)	$R_{t,typical}$	SNR (HyspIRI)	ΔR_{std} (HyspIRI)
555	7.32E−04	6.90E−02	200	3.45E−04
605	5.07E−04	5.17E−02	200	2.59E−04
625	4.16E−04	4.60E−02	200	2.30E−04
645	3.26E−04	4.11E−02	200	2.06E−04
685	1.46E−04	3.34E−02	200	1.67E−04
755	7.59E−05	2.66E−02	200	1.33E−04

as aerosol reflectance in reality does have spectral curvature following λ^{-n} where n is typically 0.7 for the global ocean (Hu, Lee, & Franz, 2012b). This scenario was used because for floating materials atmospheric correction is often difficult due to the non-zero water signal in the NIR and SWIR, making a partial atmospheric correction to derive R_{rc} more practical (Hu, 2009).

For each index, a statistical significance test was performed for the difference between the simulated *Sargassum*-water mixed spectra and other spectra. In the test, if the means differed by more than two standard deviations, then the two classes were regarded as significantly different in that index.

2.7. Spatial mixing and unmixing experiment using WV-2 data

The original WV-2 image at 2-m resolution was spatially binned (simple averaging) to 60-m resolution to evaluate whether some of the *Sargassum* features would disappear. Then, spatial unmixing was used to determine the actual *Sargassum* coverage from the coarse-resolution mixed pixels. Once a certain feature is determined to be *Sargassum*, a linear unmixing model can be used to determine the *Sargassum* proportion in each coarse pixel. In mixing water and *Sargassum*, the field-measured reflectance spectra were first convolved to MODIS bands. Then, 100,000 random pairs were made from the 50 *Sargassum* and 50 water spectra, with their relative weights (*P* and 1-*P*, see Eq. (8)) randomly selected to linearly mix the spectra in each pair. For the unmixing, a generalized linear model was fitted to 200 of the 100,000 mixed spectra (chosen randomly), then applied to all 100,000 spectra. In practice, both the water and the *Sargassum* endmembers may have spectral variability, and satellite-derived reflectance may also contain uncertainties (see above), leading to increased uncertainties from this simplified model. The model is presented here, however, to show the basic concept that unmixing pixels is possible once spectral endmembers are defined.

3. Results

In this section, qualitative analysis such as spectral inspection and visual comparison between images of different resolution is first performed. Then, quantitative results through spectral analysis and numerical simulations are presented.

3.1. Spectral inspection and interpretation

Fig. 1 shows an example of the MODIS FAI images, generated in near real-time every day from both Terra and Aqua for several regions including the GOM, central West Atlantic, and Bermuda (Hu et al., 2014; http://optics.marine.usf.edu). The image in Fig. 1 shows the coverage of the central West Atlantic from the Amazon River mouth to the north of the Lesser Antilles Islands. The image reveals many surface slicks. Spectral analyses of some of the dense features by combining the MODIS land and ocean bands (Hu, Cannizzaro, Carder, Muller-Karger, & Hardy, 2010a) did not reveal spectral curvatures in the blue-green wavelengths similar to those of *Trichodesmium*, suggesting that these dense features were not *Trichodesmium*. They could be *Sargassum* or other types of floating materials (e.g., tree leaves or small branches, marine debris, etc.). Similar spectral analyses could not be applied to other less dense slicks as the spectral signatures of various algae or materials may disappear in mixed pixels (see below).

Gower et al. (2013) examined these features using the MERIS MCI, and speculated that the regular landing of *Sargassum* on the beaches of the Lesser Antilles Islands possibly originated from the central Atlantic near the Amazon. However, MCI is based on the 709-nm MERIS band, and the large MCI values are not unique to *Sargassum*. Indeed, all floating materials on the surface would cause elevated 709-nm reflectance and thus elevated MCI values. Unfortunately, although a handful of published papers in either refereed or gray literature show field-measured *Sargassum* reflectance spectra (Dierssen et al., 2015; Suwandana, Kawamura, Sakuno, Evri, & Lesmana, 2012), neither MERIS nor MODIS is equipped with sufficient spectral bands to resolve the spectral curvature around 632 nm for *Sargassum* (Fig. 2a). Together with the coarse resolution (250 or 300 m), such a lack of spectral bands makes it difficult to spectrally fingerprint these features. Such a difficulty can be overcome with hyperspectral measurements from space-borne and airborne sensors with appropriate spatial resolutions, as shown below.

Fig. 2a shows the typical reflectance spectra of *Sargassum* in both the GOM and off Bermuda. Also shown in the figure are two representative reflectance spectra from the GOM clear and turbid waters. In addition to the common enhanced reflectance at >700 nm (similar to the reflectance for all other floating materials), there are two spectral features that could be used to differentiate *Sargassum* from other materials. The first is the local reflectance minimum around 632 nm due to the chlorophyll c (both c1 and c2) pigments. These pigments have a local absorption peak between 610 and 665 nm, with a full-width-half-maximum (FWHM) of about 25 nm and maximal absorption around 636 nm (Bidigare, Ondrusek, Morrow, & Kiefer, 1990). Such absorption properties lead to a local reflectance minimum at 632 nm (annotated by an arrow) and maxima at 620 and 647 nm. The second is the enhanced reflectance between 580 and 650 nm (outlined by the dotted circle), as compared with the reflectance of water in the same spectral region or compared with reflectance of the same feature at <550 nm. This is due to the absorption of fucoxanthin pigment between 400 and 600 nm (absorption peak around 500 nm with a FWHM of 100 nm) (Bidigare et al., 1990). The enhanced 580–650 nm reflectance is why *Sargassum* appears brownish. In contrast, although cyanobacteria such as *Trichodesmium* can also form surface mats to cause a local reflectance minimum around 625 nm (annotated by an arrow) due to the phycocyanin (PC) pigment (Dekker, 1993; Qi et al., 2014), cyanobacteria mats do not have the brownish color or enhanced reflectance in the 580–650 nm region (Fig. 2b). Furthermore, the FWHM of PC absorption (75 nm) is much wider than chlorophyll c absorption, leading to subtle difference in the local reflectance curvature. The green macroalga *U. prolifera* does not have the 632-nm feature either, and it shows enhanced reflectance in the green (~555 nm) as compared to the 580–650 nm region (Fig. 2c He et al., 2011). Likewise, the seagrass *Syringodium* does not have either the 632-nm feature or the enhanced reflectance between 580–650 nm (Fig. 2f). Other floating materials such as emulsified oil (Fig. 2d) or marine garbage (Fig. 2e) do not show the 632-nm reflectance minimum although they show enhanced reflectance between 580–650 nm as compared with reflectance in the green. Thus a reflectance minimum at 632 nm and enhanced reflectance between 580 and 650 nm should be able to discriminate *Sargassum* from other floating materials once hyperspectral data are available.

Fig. 3a shows such an example from HICO. The image was acquired on the same day, but separated by 2 h from a MODIS collection. The RGB image was generated from three bands using the HICO R_{rc} data. Sample spectra were extracted from the visually identified slick features, and are shown in Fig. 3b. To remove the residual atmospheric effects from the partially corrected R_{rc} data, the differences between the slick features and nearby water are shown in Fig. 3b. Compared with the field-collected reflectance spectra of *Sargassum* in Fig. 2a, the R_{rc} spectra of the slick feature in Fig. 3a show decreased magnitudes in all spectral range, possibly due to the fact that the 90-m HICO pixel is mixed water and *Sargassum*, or *Sargassum* is slightly submerged in water. Nevertheless, the R_{rc} spectra in Fig. 3b clearly show 1) elevated values between 580 and 650 nm and 2) local reflectance minimum around 632 nm. These are all characteristics of *Sargassum* as opposed to other floating materials, as interpreted from all endmember spectra shown in Fig. 2. Thus, without concurrent field validation, the spectral inspection revealed that at least some of the MODIS-identified FAI features in Fig. 1 are most likely *Sargassum* slicks.

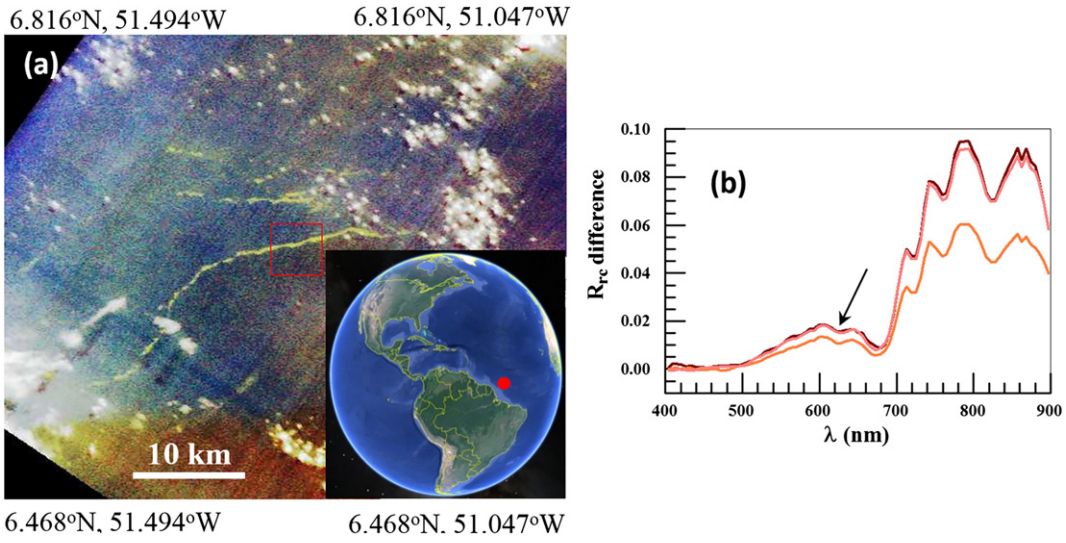

Fig. 3. (a) HICO RGB image on 1 July 2012 (12:20 GMT) showing clouds and surface slicks of suspect features. This portion of the projected HICO image covers the area 6.468°N–6.816°N and 51.494°W–51.047°W in the central West Atlantic (inset figure). Note that the image was collected on the same day as the MODIS/Terra image in Fig. 1. (b) HICO R_{rc} spectra from three pixels of the suspect feature outlined in the red box of (a), referenced against the nearby clear water. The spectral shape between 600 and 650 nm mimics that of *Sargassum* due to chlorophyll c pigment absorption (Fig. 2a).

Similar to HICO measurements, AVIRIS data collected over the northern GOM may also be used to differentiate *Sargassum* from other features. Fig. 4 shows several AVIRIS flight lines on 24 May 2010 in the west of the Mississippi Bird-Foot Delta in response to the DWH oil spill. The RGB image, generated using un-projected L_t data, shows several suspect slicks. It was unclear whether these slicks were *Sargassum*, *Trichodesmium*, or emulsified oil. Spectral analyses indicated that these slicks were not *Trichodesmium* because they did not show the typical maxima and minima in the blue-green wavelengths (Hu, Cannizzaro, Carder, Muller-Karger, & Hardy, 2010a). The slicks did not

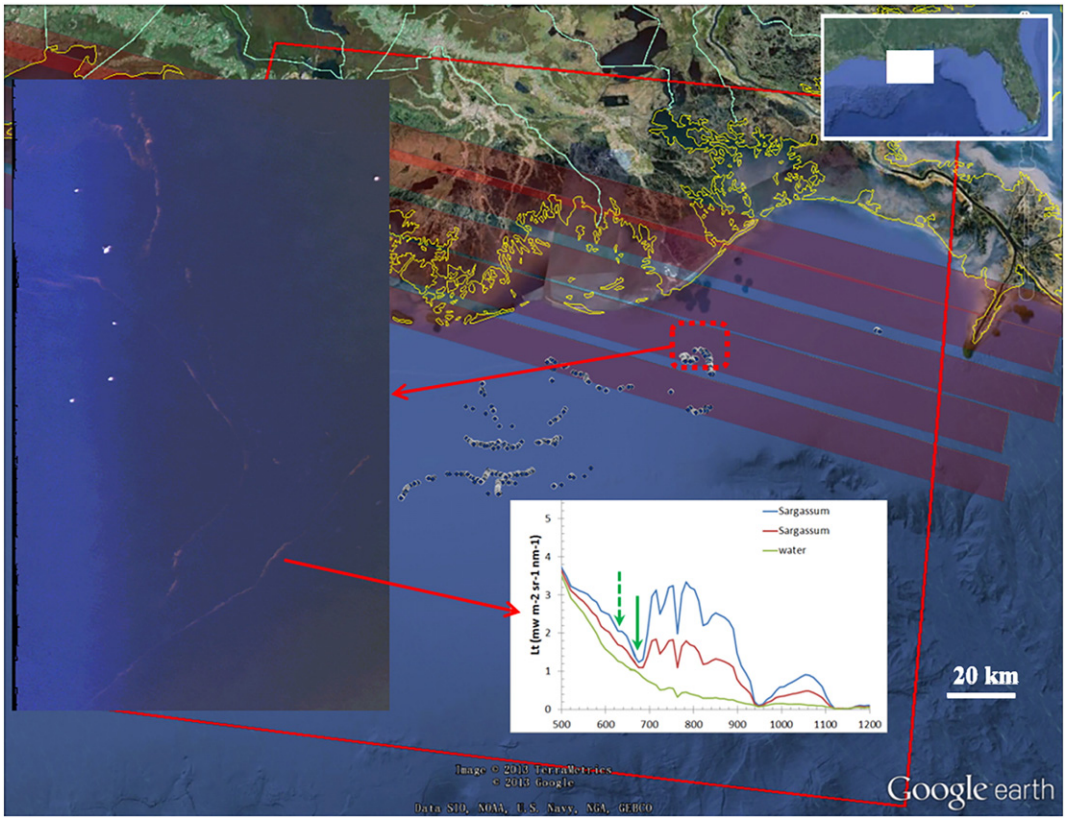

Fig. 4. AVIRIS flight lines on 24 May 2010 overlaid on the Google-Earth background image covering the west of the Mississippi Bird-Foot Delta. A portion of the one flight line is displayed to the left as an RGB image (generated using un-projected L_t data). The spectral shapes of the surface slicks were analyzed, with examples shown in the inset figure, where local minimum around 625 nm and 670 nm are annotated with the green arrows. These spectra were extracted from single pixels, but their nearby pixels showed nearly identical spectra. The red square on the background shows the footprint of the Landsat coverage, and the black/white dots denote locations of the Landsat-identified features (thought to be *Sargassum*).

appear as emulsified oil either, because they did not show the oil-specific features around 1.7 and 2.1 μm (Clark et al., 2010). Instead, two local minima around 625 nm and 670 nm were found from the spectra. In addition, compared with the spectra of nearby water, the L_t signal between 580 and 650 nm was much higher. These are all characteristics of *Sargassum*. Although the sample spectra in Fig. 4b were extracted from single pixels, their nearby pixels showed nearly identical spectra. Thus, even without field measurements, one may conclude that no other known organism or material would have such spectral shapes, and the slicks are most likely *Sargassum*.

Although the spectral shapes of the visually identified features can be used to differentiate *Sargassum* from other floating materials, it is not straightforward to establish classification rules from the AVIRIS measurements. Although the 625-nm local minimum is a unique signature for *Sargassum* (after ruling out the possibility of *Trichodesmium*), its spectral contrast is not as apparent as the 670-nm minimum, possibly due to the non-optimal band locations of the 10-nm bands and mixed pixels (see spectral analysis below). Thus, once the possibilities of *Trichodesmium* and emulsified oil are ruled out through visual inspection of the spectral shapes and the 625-nm feature is found from at least some pixels of the feature, a simple rule of $L_t(704) > L_t(675)$ can be established to delineate the slicks within this region of interest (ROI). Fig. 5 shows the results of applying such a classification rule to the ROI of the AVIRIS image. Overall, a total of 1580 AVIRIS pixels were classified as containing *Sargassum*. At a ground resolution of 12.2×12.2 m^2, this corresponds to an area of 235,167 m^2. Note that the same rule also discarded the cloud pixels. Tests of this approach (spectral analysis + ROI + simple rule) over several other cases also showed similar success. Thus, although the rule cannot be applied blindly to the entire image, the pre-processing of the image using spectral analyses and ROI can be used before the rule is applied.

In short, the hyperspectral capacity of a HICO-like or AVIRIS-like sensor would make it possible to fingerprint *Sargassum* in the remote sensing imagery. Although visual inspection is required, in the future some generalized rules may be developed to automate the process. In the absence of hyperspectral capacity, once a certain floating feature is identified using either NDVI, FAI, or MCI, three spectral bands around 600, 625, and 650 nm may be placed on satellite or airborne sensors to help identify the local spectral feature to differentiate *Sargassum* from other look-likes. The exact band centers may vary with spectral resolution (see below), however. An additional band in the green can also help differentiate *Sargassum* from *Trichodesmium* mats or floating seagrass *Syringodium*, as the latter two have enhanced reflectance in the green.

3.2. Spatial inspection and interpretation

For detecting and quantifying surface features such as *Sargassum*, spatial resolution is another major limiting factor in at least three aspects. One, an image pixel may be mixed with *Sargassum* and water (mixed pixels), leading to potential errors when using pixel numbers to estimate the total area coverage. Two, small *Sargassum* patches may be completely missed in coarse-resolution images. Finally, the mixed pixel may lose the spectral signature, making it difficult to classify the surface feature. These three aspects indicate different outcomes due to the same limitation. Here we use Landsat, AVIRIS, airborne photos, and a WV-2 image to demonstrate the first two factors, while the last factor is shown in the numerical simulation below.

Fig. 6 compares *Sargassum* coverage estimated from the same day and co-located Landsat and AVIRIS data collected on 24 May 2010. Note that the AVIRIS image is the same as shown in Fig. 5. For the common area outlined in red where Landsat pixels may contain both *Sargassum* and

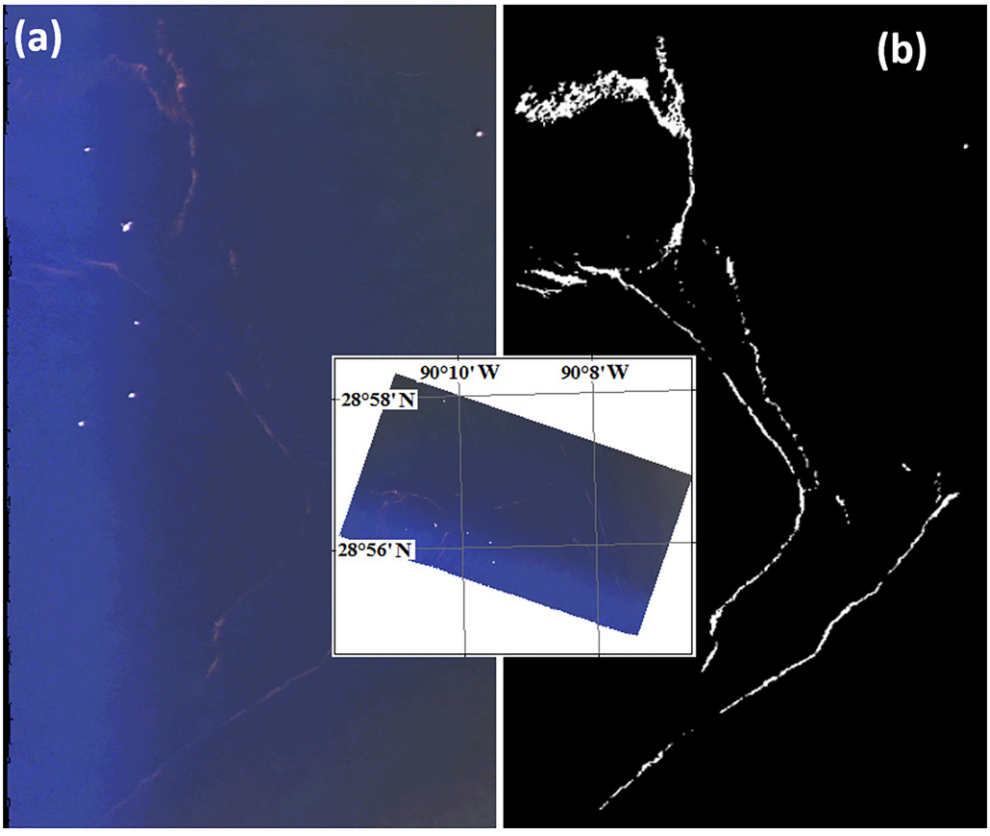

Fig. 5. (a) AVIRIS RGB image on 24 May 2010 near the Mississippi Bird-Foot Delta showing surface slicks, which were regarded as *Sargassum* according their spectral shapes. This is the same image as shown in Fig. 4. (b) Delineation of the *Sargassum* slicks using the rule of $L_t(704) > L_t(675)$ for this particular region. A total of 1580 AVIRIS pixels were classified as *Sargassum*, equivalent to $1580 \times 12.2 \times 12.2 = 235167$ m^2 in *Sargassum* coverage. The inset figure shows the location and orientation of the AVIRIS image.

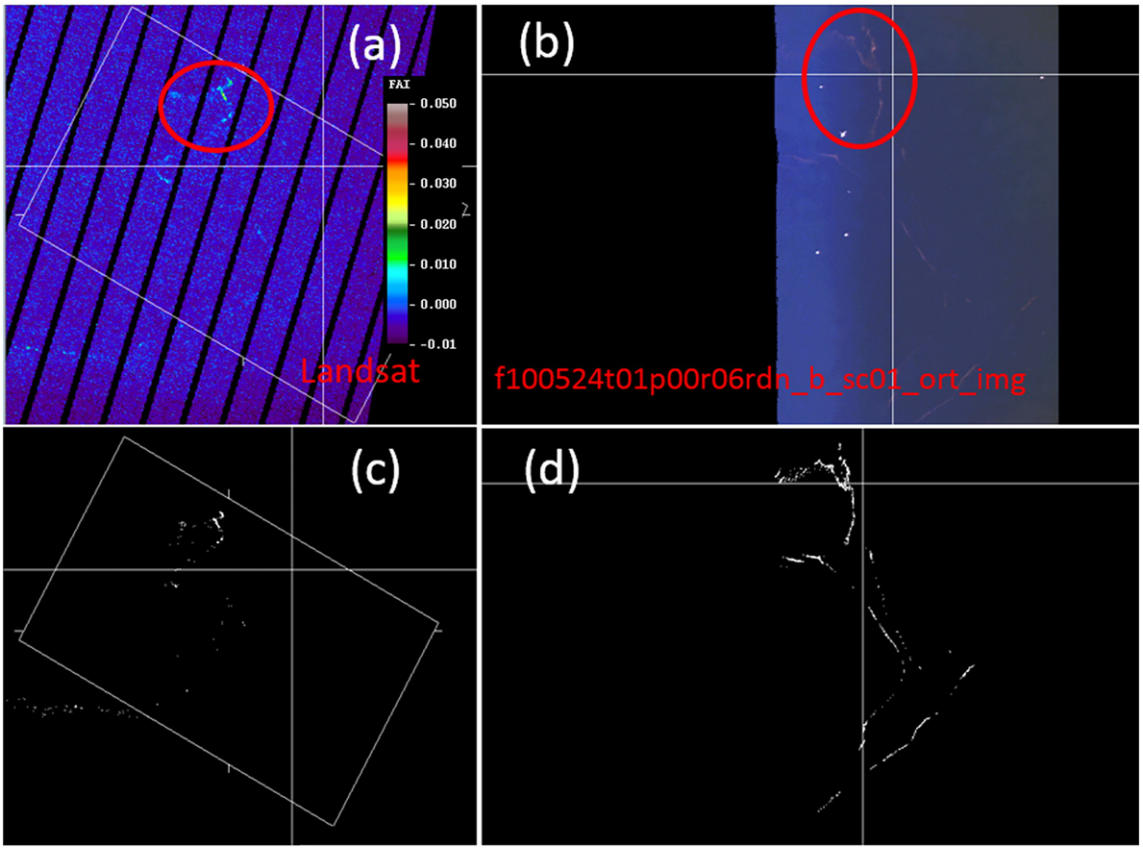

Fig. 6. (a) Landsat FAI image collected on 24 May 2010 showing surface slicks of *Sargassum*. The footprint of the entire Landsat image is shown in Fig. 4. The white rectangle shows the footprint of the corresponding AVIRIS measurement (location and orientation shown in Fig. 5). (b) AVIRIS RGB image collected on the same day (Run 06, f100524t01p00r06rdn_b_sc01_ort_img). The red circles on the two images outline common surface features where Landsat *Sargassum* pixels may be mixed with *Sargassum* and water (i.e., mixed pixels). (c) *Sargassum* pixels delineated from the Landsat image. (d) *Sargassum* pixels delineated from the AVIRIS image. Note that some of the AVIRIS-identified *Sargassum* pixels are completely missing in the Landsat image (i.e., missing pixels).

water, *Sargassum* coverage was estimated as 120 pixels × 30 m ×30 m / 0.83 = 130,120 m^2 (the factor of 0.83 is to take into account the missing Landsat pixels due to striping caused by the failure of the Scan-Line-Corrector). In comparison, *Sargassum* coverage estimated from AVIRIS was 781 pixels × 12.2 m × 12.2 m = 116,244 m^2. Thus, the ratio of the two estimates is Landsat/AVIRIS = 112%, suggesting that Landsat overestimated *Sargassum* coverage by 12% due to its coarser pixels. For the entire AVIRIS image, however, the *Sargassum* coverage from AVIRIS and Landsat measurements was estimated as 1580 pixels × 12.2 m × 12.2 m = 235,167 m^2 and 187 pixels × 30 m × 30 m / 0.83 = 202,771 m^2, respectively. The ratio of Landsat/AVIRIS *Sargassum* coverage for the entire image is 86.2%, suggesting that overall Landsat underestimated *Sargassum* coverage by 13.8% when all factors were considered (mixed pixels, coarse resolution, missing pixels).

Fig. 7 shows another example of Landsat and AVIRIS comparison in their *Sargassum* coverage estimates. The Landsat image is the same as shown in Fig. 6 but a different portion was used to correlate with AVIRIS data collected on the same day. For the area outlined in red, Landsat-based *Sargassum* coverage was estimated as 232 pixels × 30 m × 30 m = 208,800 m^2, while AVIRIS-based coverage was estimated as 1198 pixels × 12.2 m × 12.2 m = 178,310 m^2. Thus, for this common area Landsat overestimated *Sargassum* coverage by 17% (=(208,800 − 178,310) / 178,310). However, when the entire AVIRIS image was used, the *Sargassum* coverage from Landsat and AVIRIS measurements was estimated as 525 pixels × 30 m × 30 m / 0.964 = 472,500 m^2 (Landsat has ~3.6% missing pixels due to striping) and 2592 × 12.2 m × 12.2 m = 385,793 m^2, respectively. Landsat overestimated *Sargassum* coverage by 27% as compared with AVIRIS estimates.

Ideally Landsat/AVIRIS comparison should be performed for at least several other days to generate statistics. However, due to the sporadic nature of both measurements, the above two examples were the only cases where concurrent (same day) Landsat and AVIRIS were available. Based on the limited statistics from the above two examples, Landsat estimates of *Sargassum* area coverage agrees with AVIRIS to within ±30%. In other words, the 30-m resolution Landsat appears to be able to detect and quantify *Sargassum* coverage with ±30% uncertainties, if AVIRIS measurements were regarded as the "truth". However, such an uncertainty does *not* include those potential small *Sargassum* patches missed by AVIRIS due to inadequate resolution. Such possibilities were evaluated by comparing AVIRIS and concurrent airborne photographs, as shown below.

Fig. 8a shows the locations of 24 airborne photographs taken on 24 May 2010, all to the west of the Mississippi delta and covered by AVIRIS flight lines on the same day. Of the 24 photographs, 5 showed *Sargassum* mats (Fig. 8c & d). However, AVIRIS data from the same locations, after careful inspection of the spatial contrast and spectral shapes, did not reveal any suspect features. These small *Sargassum* patches were therefore completely missed by the 12-m resolution AVIRIS data. Two other cases were also examined to see whether this observation could be generalized. On 18 May 2010 and 12 July 2010, concurrent AVIRIS flight lines and airborne photos were examined. Unfortunately, of the 29 photographs taken on May 18 and 17 photos on July 12, none showed any signs of *Sargassum*.

Similar results were found from the WV-2 observations (2-m resolution) when compared with concurrent MODIS imagery (250-m resolution). Fig. 9a shows the RGB composite of the WV-2 image near Bermuda on 8 December 2009, where many slicks of *Sargassum*-like

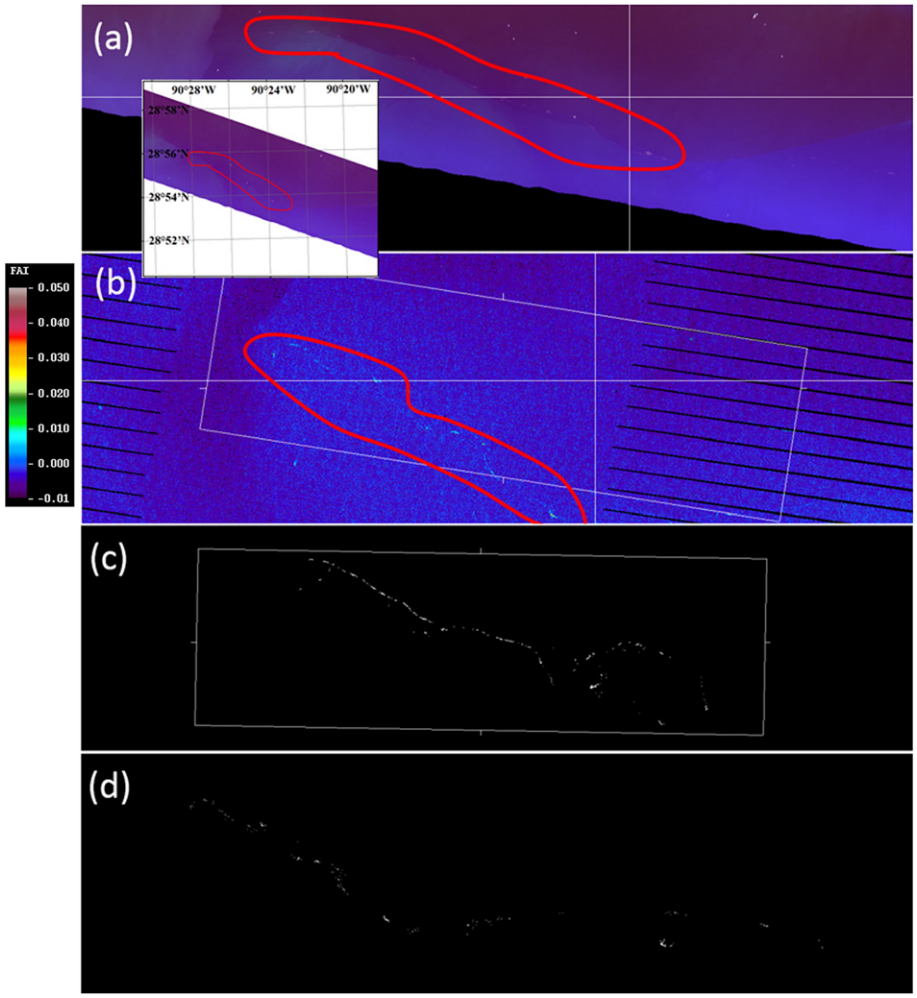

Fig. 7. (a) AVIRIS RGB image collected on 24 May 2010 (Run 05, f100524t01p00r05rdn_b_sc01_ort_img) in the west of the Mississippi Bird-Foot Delta. The areas outlined in red contain surface slicks that appear as *Sargassum*. (b). Landsat FAI image collected on the same day showing slicks in the red outlined area. The white rectangle shows the AVIRIS footprint. (c) *Sargassum* pixels delineated from the AVIRIS image. (d) *Sargassum* pixels delineated from the Landsat image. The red circles in (a) and (b) outline common surface features where both AVIRIS and Landsat *Sargassum* pixels may be mixed with *Sargassum* and water (i.e., mixed pixels, and this is why the slick features appear weak on both images). Elsewhere, some of the AVIRIS-identified *Sargassum* pixels are completely missing in the Landsat image (i.e., missing pixels).

features can be visualized. One such feature, shown in box 3, is also captured by the MODIS/Terra FAI image on the same day (Fig. 9b). However, the slicks in boxes 1 and 2 are completely missed by the 250-m resolution MODIS FAI image due to the coarse resolution, suggesting that MODIS imagery can capture only large-scale *Sargassum* slicks of at least several meters in slick width. Using a simple linear unmixing scheme, Hu (2009) estimated that the lower-detection limit of MODIS in capturing floating macroalgae slicks is 5–10 m in slick width and at least several pixels in slick length. The requirement of several pixels in slick length is to increase confidence in feature detection, as a single outlier pixel with enhanced reflectance is often treated as noise.

3.3. Spectral requirements for Sargassum detection

Recently, Dierssen et al. (2015) used the airborne Portable Remote Imaging Spectrometer (PRISM) imagery at 1-m resolution (350–1050 nm at 3.1-nm resolution, 1240 and 1610 nm at 20-nm resolution) to assess the spectral properties of *Sargassum* rafts and aggregations of seagrass (*Syringodium filiforme*) wrack in the Greater Florida Bay. Based on the inspection of the spectral reflectance, they proposed a two-step scheme to detect *Sargassum*: the floating feature is first identified using NDVI, and a 650/630 band ratio is then used to differentiate *Sargassum* from *Syingodium* because the latter does not show the spectral curvature around 630 nm.

The derivative analysis in this study identified wavelength centers at 602, 632, and 647 nm for the spectral feature around 630 nm for *Sargassum* (Fig. 2a) when the spectral resolution are 1 or 5 nm. However, when calculating the LD index, the best combinations are (602, 623, 647), (602, 622, 647), and (605, 625, 645) for the spectral resolutions of 1, 5, and 10 nm, respectively. This suggests that when the satellite sensor has continuous 5-nm bands (e.g., GEO-CAPE), the three bands should be centered at 602, 622, and 647 nm. When the satellite sensor has continuous 10-nm bands (e.g., HyspIRI), the three bands should be centered at 605, 625, and 645 nm instead.

The various indexes defined in Eqs. (3)–(6) were derived from the endmember spectra in Fig. 2 using all three resolutions, with results presented in Table 3 (note the difference in band center selections). Of all these floating materials, *Sargassum* can be differentiated unambiguously using the following step-wise rules:

1) NDVI > 0 (floating materials);
2) LD > 2×10^{-3} (spectral curvature around 630 nm to rule out the possibility of *Syringodium*, emulsified oil, and garbage);
3) RGR > 1 (to rule out the possibility of *Trichodesmium*, *Syringodium*, and *Ulva*).

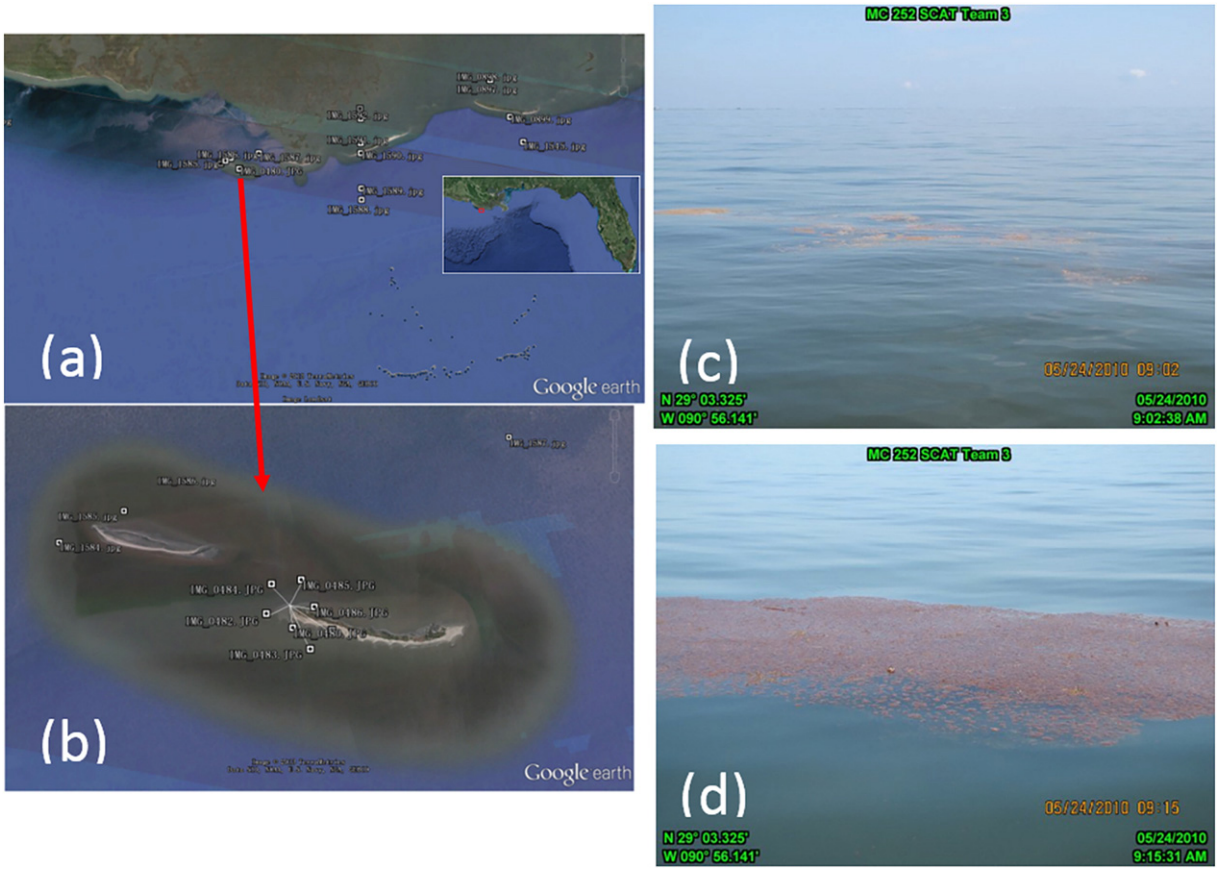

Fig. 8. (a) AVIRIS lines (horizontal strips) on 24 May 2010 overlaid in Google Earth, where Landsat-identified *Sargassum* locations are annotated as dots and airborne photo locations are annotated as squares. (b) Zoom in of 24 airborne photo locations. Note that all locations are covered by AVIRIS flight lines. (c) and (d): Airborne photos show *Sargassum* mats at 9:02 am and 9:15 am (local time), respectively. In total, 5 of the 24 photos showed *Sargassum* mats, which were completely missed by the AVIRIS measurements due to the coarser resolution.

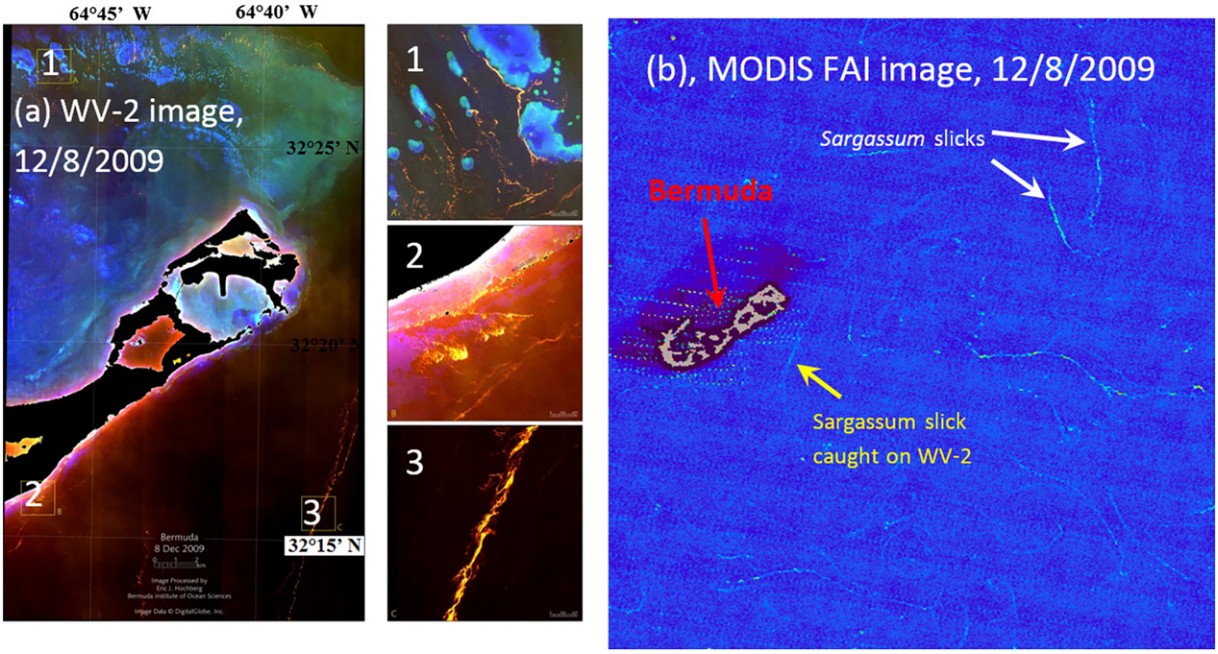

Fig. 9. (a) Color-infrared WV-2 image (2-m resolution) on 8 December 2009 around Bermuda showing various slicks thought to be *Sargassum*. The three boxes are zoomed in to the right to show the slick features. (b) MODIS/Terra FAI image (250-m resolution) on the same day shows surface slicks that are thought to be *Sargassum*. The slick annotated by the yellow arrow corresponds to the WV-2 slick in box 3.

Table 3
Spectral discrimination indexes (Eqs. (3)–(6)) calculated from endmember spectra of different floating materials (Fig. 2) for 3 resolutions. The band centers for each resolution are listed separately. *Sargassum* can be identified unambiguously using the criteria of NDVI > 0, LD > 2×10^{-3}, and RGR > 1. The individual indexes meeting these criteria are colored in red. Note that oil has higher SI and RGR than *Sargassum*, thus it is impossible to use the two indexes alone to differentiate *Sargassum* from oil.

Features	1-nm resolution bands (nm)				5-nm resolution bands (nm)				10-nm resolution bands (nm)			
	NDVI (685, 755)	LD (602, 623, 647)	RGR (555, 647)	SI (633, 646)	NDVI (685, 755)	LD (602, 622, 647)	RGR (552, 647)	SI (632, 647)	NDVI (685, 755)	LD (605, 625, 645)	RGR (555, 645)	SI (635, 645)
Sargassum	0.47	6.71E−03	1.19	1.07	0.47	6.49E−03	1.25	1.07	0.46	5.72E−03	1.21	1.05
Tricho	0.56	3.54E−03	0.77	1.01	0.56	3.50E−03	0.79	1.00	0.55	3.00E−03	0.78	1.00
Syringodium	0.77	−3.34E−03	0.48	0.73	0.77	−2.71E−03	0.49	0.71	0.76	−3.08E−03	0.52	0.79
Ulva	0.71	−1.46E−03	0.38	0.80	0.71	−1.42E−03	0.38	0.78	0.71	−1.28E−03	0.40	0.84
Oil	0.26	−1.05E−03	2.63	1.18	0.26	−9.24E−04	2.77	1.21	0.26	−1.16E−03	2.67	1.13
Garbage	0.01	−8.21E−04	1.12	1.01	0.01	−6.33E−04	1.12	1.01	0.00	−1.11E−03	1.12	1.01

For an environment free of emulsified oil and garbage, a similar set of rules through the use of SI can also be established to differentiate *Sargassum* from other floating materials:

1) NDVI > 0 (floating materials);
2) SI > 1 (to rule out the possibility of *Syringodium* and *Ulva*);
3) RGR > 1 (to rule out the possibility of *Trichodesmium* and *Ulva*).

Note that it would be difficult to use the original two-step rules proposed by Dierssen et al. (2015) (i.e., NDVI > 0, SI > 1.0) to differentiate *Sargassum* from *Trichodesmium* even in the absence of emulsified oil and garbage.

In practice, if some type of *a priori* knowledge is available, these rules may indeed be relaxed and simplified. For example, if in a certain region there is no emulsified oil or garbage (or these two possibilities can be ruled out using MCI as MCI would have low values due to their relatively smooth reflectance at >700 nm, Fig. 2d & e), a combination of NDVI and RGR would be sufficient to differentiate *Sargassum* from *Trichodesmium* or *Syringodium* or *Ulva*. Likewise, when some other possibilities are ruled out, the rules to differentiate other endmembers may be established in a similar fashion from Table 3.

One interesting result is that although the magnitude of LD for *Sargassum* decreased by 12–15% when the resolution was changed from 1 nm (or 5 nm) to 10 nm, its magnitude relative to *Trichodesmium* remained rather stable (LD ratio between the two remained to be 1.85–1.91). Therefore, spectral resolutions from 1 nm to 10 nm would perform similarly for this purpose. For the expected HyspIRI spectral coverage and resolution, the following six 10-nm bands centered at 555, 605, 625, 645, 685, and 755 are recommended for optimal performance when the 3-step rules are used to detect and differentiate *Sargassum* from other floating materials. Here both FAI (with an additional band in the SWIR, e.g., 1240 nm) and MCI can be used to replace NDVI in the above steps for their tolerance to the environmental perturbations. If for any reasons during the engineering design the 10-nm bands were centered at different wavelengths, although the influence on the NDVI and RGR would be negligible, the sensitivity of using LD for *Sargassum* discrimination may be degraded. For example, if the three band centers are placed at 600, 620, and 650 nm, LD for *Sargassum* and *Trichodesmium* would be 4.82 and 3.32×10^{-3}, respectively. Not only is the magnitude of LD much smaller (from 5.72 to 4.82, a 16% decrease), but the LD ratio between *Sargassum* and *Trichodesmium* is also decreased significantly (from 1.91 to 1.45, a 24% reduction). Clearly, even with a fixed spectral resolution, the band centers need to be chosen carefully.

3.4. Spatial detection limit

Using the simulation methods detailed in Section 2.6, the detection limits are listed in Table 4. For brevity, only the results from the second

Table 4
Three indexes estimated with different percentage of water (for both Chla = 0.14 mg m^{-3} (a) and 0.8 mg m^{-3} (b)) mixed with other floating materials, where ΔR_{std}(HyspIRI) of Table 2 was used to simulate the noise and then added to the mixed reflectance spectra (Eq. (8)). Wat: water; Sar: *Sargassum*; Tri: *Trichodesmium*; Syr: *Syringodium*; Gar: Garbage. All values shown in the tables are the mean values from 1000 simulations, except that the columns of "Sar" are the mean values minus 2 times of standard deviations. At 80% water mixing, all three indexes of *Sargassum* are significantly greater than their corresponding thresholds (NDVI > 0, LD > 0, and RGR > 1), suggesting that a 20:80 *Sargassum*:water mixture can still be spectrally discriminated. For turbid waters (Chla = 0.8) this detection limit is 30:70 for *Sargassum*:water.

Wat (%)	NDVI						LD						RGR					
	Sar	Tri	Ulv	Syr	Gar	Oil	Sar	Tri	Ulv	Syr	Gar	Oil	Sar	Tri	Ulv	Syr	Gar	Oil
Chla = 0.14 mg m^{-3} for water endmember																		
95%	0.10	0.03	0.12	0.24	−0.0063	0.08	−1.66E−04	1.77E−04	−6.78E−06	−9.64E−05	2.43E−06	1.60E−04	0.84	0.78	0.76	0.76	0.87	1.03
90%	0.18	0.06	0.21	0.37	−0.0038	0.12	1.81E−04	2.83E−04	−7.97E−05	−2.60E−04	−6.33E−05	2.52E−04	0.91	0.77	0.74	0.74	0.92	1.22
85%	0.23	0.09	0.28	0.45	−0.0023	0.14	4.97E−04	3.98E−04	−1.47E−04	−4.18E−04	−1.22E−04	3.51E−04	0.96	0.76	0.71	0.72	0.95	1.38
80%	0.26	0.11	0.33	0.50	−0.0014	0.16	8.66E−04	5.21E−04	−2.04E−04	−5.64E−04	−1.71E−04	4.60E−04	1.00	0.76	0.69	0.70	0.98	1.51
75%	0.29	0.13	0.37	0.54	−0.0005	0.16	1.19E−03	6.16E−04	−2.91E−04	−7.41E−04	−2.50E−04	5.39E−04	1.04	0.75	0.68	0.69	1.00	1.63
70%	0.31	0.15	0.40	0.56	0.0001	0.17	1.52E−03	7.47E−04	−3.41E−04	−8.82E−04	−2.92E−04	6.55E−04	1.07	0.74	0.66	0.68	1.02	1.73
65%	0.33	0.17	0.43	0.59	0.0005	0.18	1.89E−03	8.66E−04	−4.04E−04	−1.03E−03	−3.46E−04	7.58E−04	1.10	0.74	0.65	0.67	1.03	1.81
60%	0.34	0.19	0.45	0.60	0.0009	0.18	2.22E−03	9.85E−04	−4.65E−04	−1.19E−03	−3.99E−04	8.62E−04	1.12	0.73	0.64	0.66	1.04	1.89
55%	0.35	0.20	0.47	0.62	0.0013	0.18	2.59E−03	1.10E−03	−5.32E−04	−1.34E−03	−4.58E−04	9.61E−04	1.14	0.73	0.63	0.66	1.05	1.96
Chla = 0.8 mg m^{-3} for water endmember																		
95%	0.09	0.01	0.11	0.23	−0.0170	0.08	−1.03E−04	2.40E−04	5.92E−05	−3.08E−05	6.70E−05	2.24E−04	0.77	0.72	0.70	0.70	0.80	0.93
90%	0.17	0.05	0.20	0.36	−0.0122	0.12	2.23E−04	3.51E−04	−1.16E−05	−1.92E−04	5.16E−06	3.21E−04	0.84	0.72	0.68	0.69	0.85	1.11
85%	0.22	0.08	0.27	0.44	−0.0091	0.14	6.04E−04	4.64E−04	−8.01E−05	−3.51E−04	−5.57E−05	4.18E−04	0.89	0.71	0.67	0.68	0.90	1.26
80%	0.26	0.10	0.32	0.49	−0.0067	0.15	8.82E−04	5.56E−04	−1.69E−04	−5.29E−04	−1.36E−04	4.95E−04	0.94	0.71	0.66	0.67	0.93	1.40
75%	0.28	0.12	0.36	0.53	−0.0048	0.16	1.25E−03	6.84E−04	−2.22E−04	−6.73E−04	−1.82E−04	6.07E−04	0.98	0.71	0.65	0.66	0.96	1.52
70%	0.30	0.14	0.39	0.56	−0.0035	0.17	1.56E−03	7.97E−04	−2.92E−04	−8.32E−04	−2.42E−04	7.04E−04	1.02	0.71	0.64	0.66	0.98	1.62
65%	0.32	0.16	0.42	0.58	−0.0025	0.17	1.94E−03	8.98E−04	−3.70E−04	−1.00E−03	−3.14E−04	7.91E−04	1.05	0.71	0.63	0.65	1.00	1.72
60%	0.34	0.18	0.45	0.60	−0.0016	0.18	2.26E−03	1.02E−03	−4.34E−04	−1.15E−03	−3.66E−04	8.95E−04	1.08	0.71	0.62	0.65	1.02	1.80
55%	0.35	0.19	0.47	0.62	−0.0009	0.18	2.62E−03	1.13E−03	−5.00E−04	−1.31E−03	−4.27E−04	9.93E−04	1.10	0.71	0.61	0.64	1.03	1.88

scenario (i.e., the partially corrected R_{rc} data with projected HyspIRI SNRs, column 5 of Table 2) are presented here. Results from the first scenario (i.e., standard ocean color atmospheric correction and surface reflectance uncertainties estimated from SeaWiFS, column 2 of Table 2) are very similar.

First, a surface floating feature due to *Sargassum* can be easily detected in the NDVI image. In both scenarios, NDVI of the mixed pixel is significantly >0 as long as the *Sargassum* proportion of the pixel is >0.7% when the water endmember has Chla of 0.14 mg m^{-3} and >1.1% when the water endmember has Chla of 0.8 mg m^{-3}. In other words, for a 60-m resolution sensor and clear-water background, a surface slick of >0.4 m in width and >180 m in length (the requirement for >3 pixels in length is because a single-pixel anomaly is often treated as an image outlier and thus discarded) can clearly show up in the NDVI imagery as an anomaly. For more turbid waters (Chla = 0.8 mg m^{-3}) the detection limit is 0.7 m in width and >180 m in length. Hu (2009) used MODIS-derived spectra as endmember of *Ulva*, and estimated that the detection limit was 2–4% of the MODIS 250-m pixel (i.e., 5–10 m in slick width). Such an estimate agrees well with the visual inspection of the image pair of WV-2 (2-m resolution) and MODIS in Fig. 9, where the MODIS FAI image could barely reveal slicks caught by WV-2 (several meters in slick width). The endmember spectra in Hu (2009) were perhaps underestimated in magnitude due to either mixed MODIS pixels or slightly submerged *Ulva* in water, resulting in an overestimate of the detection limit. In other words if MODIS endmember spectra of *Ulva* completely exposed to air were used, the 250-m imagery could reveal *Ulva* slicks of 2–5 m in width if they were also exposed to air. For the same argument, if *Sargassum* (or other floating materials) is submerged in water for only 15 cm, the enhanced NIR reflectance would decrease by $\exp(-2.5\ m^{-1} \times 0.15\ m \times 2) = 47\%$ (here 2.5 m^{-1} is the water absorption coefficient at 752 nm, and 2 is to take into account the 2-way water attenuation), and the detection limit is decreased to 1.1%/47% = 2.3%. Another possible reason to lose the detection sensitivity is the atmospheric attenuation that was not considered in the simulation. For small bright features, atmospheric attenuation is higher than diffused water surface, resulting in a loss of surface reflectance and the spatial contrast. Therefore, with all these potential factors taken into account, detecting a surface *Sargassum* slick without spectral discrimination is easy with NDVI (and also with FAI) even if the feature is sufficiently small compared to the pixel size (e.g., 1–2%).

Second, once the slick is detected in the NDVI imagery, differentiating *Sargassum* from other floating materials requires a much larger proportion of *Sargassum* in the mixed pixel. Table 4a shows that in order to tell whether a detected slick is *Sargassum* from the 3-step rules (NDVI > 0, LD > 0, RGR > 1), the minimum *Sargassum* proportion of a pixel (P_{min}) was 20% (80% water). For turbid waters P_{min} of *Sargassum* increased to 30% (70% water) (Table 4b). Note that such rules did not rule out garbage or oil as they both show LD > 0 and RGR > 1 at these detection limits. However, without *a priori* knowledge of the environment, a slight adjustment of the LD threshold, for example LD > 5×10^{-4}, can easily rule out these two possibilities. Indeed, because both garbage and emulsified oil showed continuously high reflectance in the NIR (as opposed to a local peak between 700 and 730 nm), they would show relatively lower MCI values than *Sargassum*, and the use of MCI could also rule out these two possibilities.

In summary, the simulation results suggest that for nearly all cases considered using different atmospheric correction schemes and noise considerations, although it is very easy to detect a small surface floating slick (P_{min} ~ 1–2% of pixel size) in the NDVI (and possibly FAI or MCI) imagery, spectral discrimination between *Sargassum* and other floating materials requires a much higher P_{min} (20–30%), corresponding to 12–18 m slick width for the HyspIRI 60-m resolution data.

3.5. Spatial mixing and unmixing experiment using WV-2 data

Fig. 10 shows the comparison between the original WV-2 image at 2-m resolution and the spatially binned (simple averaging) image at 60-m resolution. This is the same image as shown in Fig. 9a (box 1). Many of the small slicks observed in (a), as outlined in red, disappeared in the reduced-resolution image in (b). However, the large slicks are retained in (b), indicating that HyspIRI would be able to map large *Sargassum* mats near Bermuda, which is potentially useful to understand *Sargassum* ecosystem dynamics.

The spatial averaging in Fig. 10 can be reversed to determine the actual *Sargassum* coverage from the coarse-resolution mixed pixels. Fig. 11A shows the field measured *Sargassum* and water spectra convolved to MODIS bands, while Fig. 11B shows that the unmixing model worked fairly well in predicting the proportion of *Sargassum* in the mixed pixels, with an estimated uncertainty of ±5%. In practice, both the water and the *Sargassum* end-members will have spectral

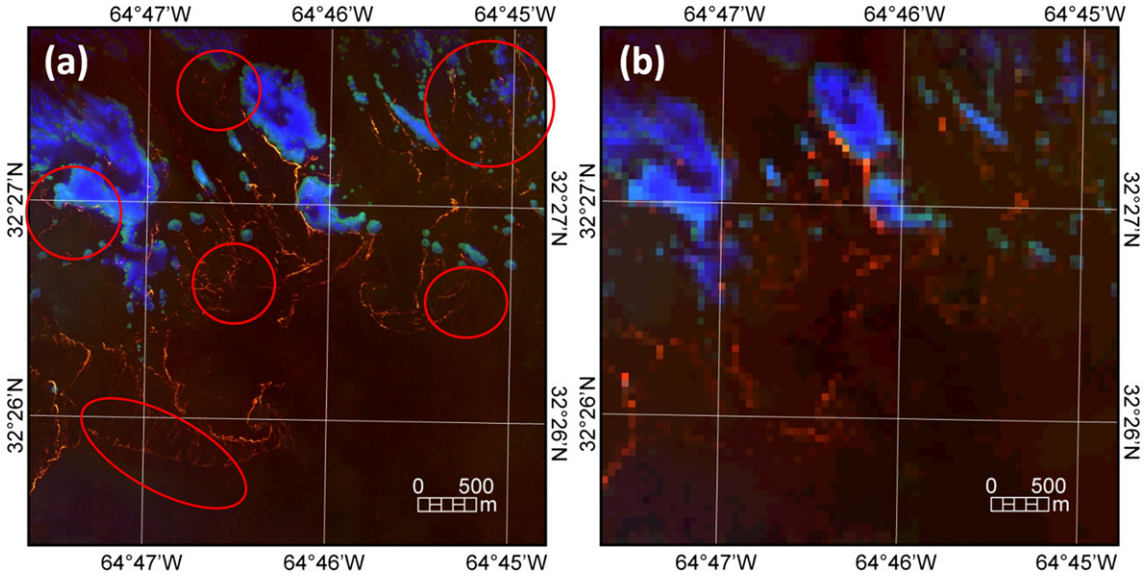

Fig. 10. (a) WV-2 RGB image at 2-m showing many *Sargassum* rafts around coral reefs near Bermuda. This is the same image as in box 1 of Fig. 9a. (b) The same image after binning to 60-m resolution. Many of the small rafts in (a), some of which are outlined in red circles, disappeared in (b), yet large rafts can still be visualized at 60-m resolution.

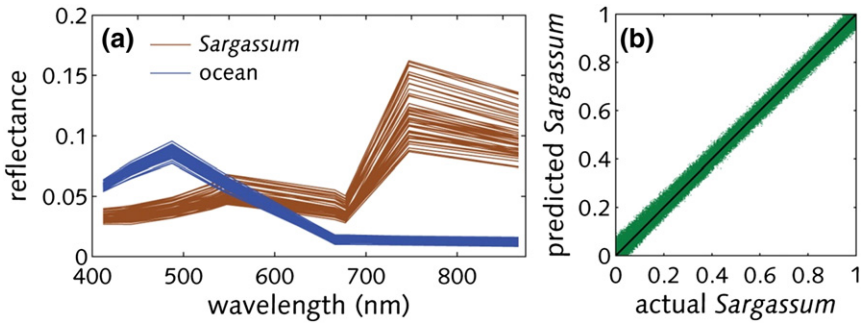

Fig. 11. A. Reflectance spectra of the ocean (sandy bottom at ~10 m depth, blue lines) and floating *Sargassum* (brown lines) measured off Bermuda, convolved to MODIS ocean wavebands. The reflectance spectra are shown in Fig. 2b. B. Results of spectral unmixing for 100,000 modeled ocean–*Sargassum* mixtures using a generalized linear model. Thick black line shows 1:1 relationship between actual and predicted *Sargassum* proportions.

variability, leading to increased uncertainties in the unmixing results than shown in Fig. 11b. Such an uncertainty, however, should not be interpreted as the detection limit of mixed pixels as shown in Section 3.4, but an uncertainty in the estimated mixing ratio as a result of many spectral endmembers used in the model. On the other hand, the unmixing is possible to reduce uncertainties in the coverage estimates *only if* the coarse-resolution pixel can be delineated as containing floating materials (i.e., proportion > P_{min}). Nevertheless, the model demonstrates the feasibility of accurate estimates of *Sargassum* coverage and possibly biomass, once the spectra of the two end-members (*Sargassum* and water) are known and the parameter of biomass per area is determined from field measurements.

4. Discussion

4.1. Proposed steps to detect and quantify Sargassum from space

The spectral analyses clearly showed that in an unknown ocean environment discrimination of *Sargassum* from other floating materials would rely on the unique reflectance trough around 632 nm, together with other spectral characteristics (e.g., enhanced reflectance between 580–650 nm). Indeed, such a reflectance trough has also been reported in Dierssen et al. (2015) from field measurements and by several airborne missions. In addition to the PHILLS measurements over the Florida Keys (Szekielda et al., 2010), Marmorino, Miller, Smith, and Bowles (2011) used a Compact Airborne Spectro-graphic Imager (CASI) on an aircraft to measure hyperspectral signal between 400 and 1000 nm from *Sargassum* rafts off SE Florida, and showed a spectral trough around 625 nm. Mehrtens et al. (2009) used an AISA Eagle (AWI) hyperspectral sensor (400–970 nm, 2.9 nm) on a motor glider to measure *Sargassum* and other seaweed rafts near the island of Helgoland (Germany, North Sea), and also reported a spectral trough around 625 nm. Thus, a set of rules can be established to utilize such spectral features for *Sargassum* discrimination.

However, the above calculations and results did not consider several other important factors when satellite total reflectance (R_t) data are used for image processing. These factors include masking of clouds and severe sun glint; neither is trivial (Hu, 2009). Cloud detection in the standard ocean color data processing relies on an NIR band, based on the principle that cloud reflectance in the NIR is higher than from cloud-free ocean surface. However, all floating materials would also lead to enhanced NIR (and also SWIR) reflectance, thus making this cloudmasking approach invalid. Other approaches have used band ratios and ancillary information to improve cloud detection (see comparison in (Barnes & Hu, 2013)), yet each cloud detection scheme has its own strengths and weaknesses. Cloud detection as well as sun glint masking and atmospheric correction are still active research areas. For the purpose of *Sargassum* detection in this study, it is assumed that masking of clouds and severe sun glint can be achieved using algorithms established in the literature, resulting in either fully atmospherically corrected surface reflectance (R) or partially corrected R_{rc}, from which the detection scheme can start. Fig. 12 shows a schematic flow chart of the various steps in this entire process.

In such a process, the thresholds need to be first determined, using either simulations as shown above (but with more realistic *Sargassum* and water endmembers for the specific region) or field experiments. Then, if the proportion of the detected feature is <the detection limit for spectral discrimination, the process will stop after the spatial unmixing. This, however, does not necessarily mean that the detected feature cannot be identified because some *a priori* knowledge of the environment may be available to assist image interpretation.

4.2. Implications for data interpretation and sensor/algorithm design

First, detecting surface floating materials is primarily limited by sensor spatial resolution. This appears to be intuitive even without investigation. However, the image comparison here presented visual evidence, and the simulation further provided numerical limits. The results showed that it is possible to detect a floating slick as long as the partial coverage is >1–2% (note: the partial coverage needs to be significantly higher (20–30%) in order to spectrally discriminate the feature without *a priori* knowledge of the environment) of the mixed pixel, regardless of

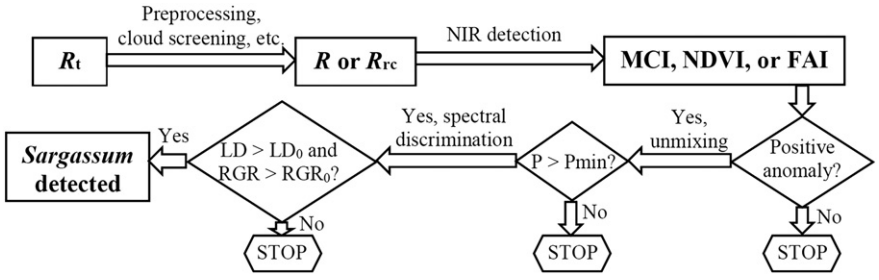

Fig. 12. Schematic flow chart showing the steps in detecting *Sargassum* from satellite measurements. LD_0 and RGR_0 are the threshold values to differentiate *Sargassum* from other floating materials.

a full or partial atmospheric correction. This is a conservative estimate that takes into account the possibility that the floating materials may be submerged to a shallow depth (e.g., 15 cm). Smaller patches of floating materials could also be captured if they are fully exposed to air. This is qualitatively demonstrated by the image comparison between various resolutions. There are cases when the small *Sargassum* patches are completely missed by the coarse-resolution pixels. Detecting these patches would require another sensor with higher resolution. Yet sensors with higher resolution typically have smaller footprint and therefore cannot be used for routine monitoring. On the other hand, it is highly desirable to have accurate knowledge of total *Sargassum* biomass or coverage in the GOM and Atlantic. Gower et al. (2006, 2011) used MERIS 300-m and 1.2-km data to estimate the total coverage, yet the coarse resolution must have missed many small patches. The current study confirms this speculation. With the Landsat 30-m resolution, most of the airborne-identified *Sargassum* patches (in the order of meter or sub-meter in size) were missed. Even with the AVIRIS 12-m resolution, the airborne-identified *Sargassum* patches were still missed. The small patches may be as important as those large *Sargassum* slicks (which showed up in MERIS or MODIS imagery) for local ecology and for tracing eddies and eddy fronts, and they may also contribute to a significant portion of the total biomass in the GOM and Atlantic. Unfortunately it is currently impossible to estimate how much *Sargassum* is undetected in coarse-resolution satellite imagery due to lack of complete coverage of finer-resolution (e.g., airborne photo) data. It is speculated that, however, once the total coverage is estimated independently by both the Landsat and airborne observations with sufficiently large coverage, a statistical relationship might be established to scale Landsat observations to result in an improved estimate of total *Sargassum* coverage.

With its proposed 19-day cycle and a swath width comparable to Landsat, the HyspIRI mission will provide cloudfree data only occasionally, thus not well suitable for routine monitoring of any fast-changing features. However, its advantage over Landsat sensor series is twofold. One, its SNRs are much higher than Landsat TM and ETM+, thus providing a better capacity for capturing small patches. SNR of ETM+ under typical radiance input over the ocean is ~70:1 at 565 nm and ~41:1 at 640 nm (Hu, Feng, et al., 2012a). SNR of the new Landsat OLI was estimated to be 220:1 at 565 nm and 80:1 at 750 nm (Pahlevan et al., 2014), almost the same as with HICO (Lucke et al., 2011). In the simulations the SNRs of HyspIRI were assumed to be 200:1 for all spectral bands over typical clear water targets. These are significantly higher than the 60:1 SNRs of AVIRIS for the red and NIR bands. Even if this requirement could not be fully met and the SNR in the red and NIR bands were comparable to those of the OLI and HICO, its sensitivity would still be much higher than that of Landsat ETM+. In this case of course the detection limit provided in Table 4 will need to be revisited. With the OLI in orbit since February 2013, it should be useful to compare concurrent and collocated OLI and ETM+ imagery to determine how much more *Sargassum* OLI may detect over ETM+ with the enhanced SNR.

Second, the optimal band centers have been determined through derivative analysis and iterative index calculations for 3 resolutions (1, 5, and 10 nm), and some of them are not multiples of 5 or 10-nm. For example, at 5-nm resolution, the optimal band centers to calculate LD are 602, 622, and 647 nm instead of 600, 625, and 650 nm. Furthermore, when atmospheric effects are considered, it is better to choose 647 than 652 nm to avoid the water vapor absorption between 645–660 nm (Gordon, 1993). The band centers of 605, 625, and 645-nm for the 10-nm resolution sensor provide new information to the band recommendations by Lee, Carder, Arnone, and He (2007), who proposed 615, 635, and 665 nm with 10-nm bandwidth in the spectral region of 600–670 nm. That study used a library of water reflectance spectra that did not include *Sargassum* or other floating materials. Likewise, the spectral reconstruction scheme of Lee, Shang, Hu, and Zibordi (2014) also did not consider these floating materials. Whether the spectral characteristics of these floating materials can be reconstructed using the proposed bands requires further analysis.

Third, the stepwise rule is to discriminate *Sargassum* from *all* other floating materials listed in this study. Often in an environment some endmembers can be ruled out to simplify the rule. For example, in the GOM although emulsified oil could be present in a limited region and limited time (e.g., the DWH case), its occurrence is rare and for most cases it can be ruled out. Garbage patches have been reported in the Pacific and Atlantic, but not in the GOM, thus could be ruled out as well. *Ulva* blooms in the GOM have not been reported either. Then, one only needs to discriminate *Sargassum* from the other two endmembers that are also commonly found in the GOM: *Trichodesmium* and *Syringodium*. The RGR index should be effective in discriminating them, as the latter two have reflectance peaking around 550 nm instead of 580–650 nm for *Sargassum*. Such a simplified rule has significant implications on the existing sensors such as MERIS and MODIS. The MERIS 620-nm band and MODIS 645-nm band may be used to derive a sensor-specific RGR to differentiate *Sargassum* from the other two once the features are delineated using either MERIS MCI or MODIS FAI. This simplified approach may be tested over known bloom cases. Similarly, although most analyses here were focused on *Sargassum*, the general approach could be extended to other floating materials, with similar stepwise rules established through Tables 3–4 and Fig. 12. For the same argument, because other brown algae also have similar spectral curvature around 630 nm (Hochberg et al., 2003), if these types of brown algae also occur in surface waters of a region where *Sargassum* is to be detected, it would be extremely difficult to differentiate *Sargassum* from them.

Finally, the sensitivity simulations are based on the spectral endmembers provide in Fig. 2. In reality, although the spectral shapes of the floating materials are unlikely to change, their magnitude can vary. More importantly, there were only two water endmembers used in the simulation, while the water spectra can change substantially in both shape and magnitude (Lee et al., 2007, 2014). For example, for sediment-rich waters the reflectance may peak around 600–640 nm (brownish). The RGR index would then be useless to separate *Sargassum* from this type of background water. For these types of situations, the simulations may be revisited to account for more realistic water endmembers. The general approach, on the other hand, should still be applicable not only to *Sargassum* but also all other floating materials.

5. Conclusion

Various marine organisms and materials floating on the sea surface can cause enhanced reflectance in the NIR, making discriminating and quantifying *Sargassum* difficult. This study analyzed the spectral characteristics of the field measured reflectance spectra of *Sargassum*, *Trichodesmium*, *Syringodium*, *Ulva*, garbage, and emulsified oil, and used multi-sensor comparison and numerical simulations to address the spectral and spatial requirements of satellite sensors in order to detect, discriminate, and quantify *Sargassum*. Spectral regions and spectral bands are identified to differentiate *Sargassum* from other look-alikes at different spectral resolutions (1, 5, and 10 nm). Once these spectral bands are available from airborne or future satellite missions such as HyspIRI, a stepwise rule using several indexes can fingerprint the *Sargassum* pixels. Currently, in the absence of several spectral bands between 580 and 650 nm on the multi-band sensors such as MODIS and MERIS, the use of the RGR index in addition to MCI (or NDVI or FAI) may be able to differentiate *Sargassum* from *Syringodium* (or *Trichodesmium*) in an environment free of emulsified oil and garbage. However, spatial resolution is another major limiting factor not only for the coarse-resolution MODIS or MERIS sensors, but also for the higher-resolution Landsat and HyspIRI sensors. Nevertheless, the HyspIRI sensor at 60-m resolution with its hyperspectral capacity and expected SNRs (200:1) would be able to detect and quantify (through

linear unmixing) *Sargassum* slicks of >1 m in width and more than 180 m in length, although spectral fingerprinting using the proposed scheme requires about 12–18 m slick width. Such a capacity, when combined with other sensors with lower-resolutions (both spectral and spatial) but more synoptic coverage, will greatly enhance our ability to map *Sargassum*, estimate total biomass, and help understand open- and coastal-ocean ecosystem dynamics.

Notations

DWH	Deepwater Horizon
GOM	Gulf of Mexico
NEGOM	Northeast Gulf of Mexico
AVIRIS	Airborne Visible/Infrared Imaging Spectrometer
CASI	Compact Airborne Spectro-graphic Imager
GEO-CAPE	Geostationary Coastal and Air Pollution Events
HICO	Hyperspectral Imager for the Coastal Ocean (2009–2014)
HyspIRI	Hyperspectral Infrared Imager
MERIS	Medium Resolution Imaging Spectrometer (2002–2012)
MODIS	Moderate Resolution Spectroradiometer (1999 — on Terra; 2002 — on Aqua)
OLI	Operational Land Imager (on Landsat 8, 2013–present)
PHILLS	Portable Hyperspectral Imager for Low-Light Spectroscopy
PRISM	Portable Remote Imaging Spectrometer
SeaWiFS	Sea-viewing Wide Field-of-view Sensor (1997–2010)
WV-2	WorldView-2
CDOM	Colored Dissolved Organic Matter (CDOM)
Chla	Chlorophyll a concentration (mg m^{-3})
F_o	Annual mean solar constant (mW cm^{-2} μm^{-1})
L	Radiance (mW cm^{-2} μm^{-1} sr^{-1})
R	Surface reflectance (dimensionless)
R_{rs}	Surface remote sensing reflectance (sr^{-1})
R_{rc}	Rayleigh-corrected reflectance (dimensionless)
NIR	Near infrared
SWIR	Shortwave infrared
FAI	Floating Algae Index
LD	Line Depth
MCI	Maximum Chlorophyll Index
NDVI	Normalized Difference Vegetation Index
RGR	Red/Green Ratio
SI	*Sargassum* Index

Acknowledgment

This work was supported by the U.S. NASA through its Ocean Biology and Biogeochemistry program, Gulf of Mexico program, Water Quality program, and through its support to the Science Definition Teams for planning future satellite missions of GEO-CAPE and HyspIRI. The analyses presented were also funded in part by NOAA as part of the 'Deepwater Horizon' oil spill Natural Resource Damage Assessment, and by the BP/Gulf of Mexico Research Initiative through C-IMAGE. We thank the NASA GSFC, European Space Agency, USGS, NASA JPL, DigitalGlobe, Inc., the U.S. Naval Research Lab, the U.S. NOAA, for providing MODIS, MERIS, Landsat, AVIRIS, WV-2, and HICO data and digital photos, respectively. We also thank Dr. Hongtao Duan and Mr. Daniel Sensi for their help in collecting *Sargassum* reflectance spectra in the Gulf of Mexico and marine garbage reflectance spectra in Tampa Bay, respectively. Four anonymous reviewers provided valuable comments to help improve this manuscript, whose effort is also appreciated.

References

Anthony, E. J., Vanhee, S., & Ruz, M. -H. (2006). Short-term beach–dune sand budgets on the North Sea coast of France: Sand supply from shoreface to dunes, and the role of wind and fetch. *Geomorphology*, *81*, 316–329.

Barnes, B. B., & Hu, C. (2013). A hybrid cloud detection algorithm to improve MODIS sea surface temperature data quality and coverage over the Eastern Gulf of Mexico. *IEEE Transactions on Geoscience and Remote Sensing*, *51*, 3273–3285.

Bidigare, R. R., Ondrusek, M. E., Morrow, J. H., & Kiefer, D. A. (1990). In-vivo absorption properties of algal pigments. *Ocean Optics X. SPIE. Orlando '90, 16–20 April: International Society for Optics and Photonics*. (pp. 290–302).

Clark, R. N., Swayze, G. A., Leifer, I., Livo, K. E., Kokaly, R., Hoefen, T., et al. (2010). *A method for quantitative mapping of thick oil spills using imaging spectroscopy. US Geological Survey Open-File Report, 1167*. (pp. 1–51), 1–51.

Council, S. A. F. M. (Ed.). (2002). *Fishery management plan for pelagic Sargassum habitat of the South Atlantic region* (pp. 228) (http://www.safmc.net/Portals/6/Library/FMP/Sargassum/SargFMP.pdf).

Dekker, A. G. (1993). *Detection of optical water quality parameters for eutrophic waters by high resolution remote sensing* (pp. 237). Netherlands: Vrije Universiteit.

Devred, E., Turpie, K. R., Moses, W., Klemas, V. V., Moisan, T., Babin, M., et al. (2013). Future retrievals of water column bio-optical properties using the Hyperspectral Infrared Imager (HyspIRI). *Remote Sensing*, *5*, 6812–6837.

Dierssen, H. M., Chlus, A., & Russell, B. (2015). Hyperspectral discrimination of floating mats of seagrass wrack and the macroalgae *Sargassum* in coastal waters of Greater Florida Bay using airborne remote sensing. *Remote Sensing of Environment*, *167*, 247–258.

Fishman, J., Iraci, L., Al-Saadi, J., Chance, K., Chavez, F., Chin, M., et al. (2012). The United States' next generation of atmospheric composition and coastal ecosystem measurements: NASA's Geostationary Coastal and Air Pollution Events (GEO-CAPE) Mission. *Bulletin of the American Meteorological Society*, *93*, 1547–1566.

Gao, B. -C. (1993). An operational method for estimating signal to noise ratios from data acquired with imaging spectrometers. *Remote Sensing of Environment*, *43*, 23–33.

Gao, B. -C., Montes, M. J., Ahmad, Z., & Davis, C. O. (2000). Atmospheric correction algorithm for hyperspectral remote sensing of ocean color from space. *Applied Optics*, *39*, 887–896.

Garcia-Pineda, O., MacDonald, I., Hu, C., Svejkovsky, J., Hess, M., Dukhovskoy, D., et al. (2013). Detection of floating oil anomalies from the Deepwater Horizon oil spill with synthetic aperture radar. *Oceanography*, *26*, 124–137.

Gordon, H. R. (1993). *Radiative transfer in the atmosphere for correction of ocean color remote sensors*. Ocean colour: Theory and applications in a decade of CZCS experience. Springer, 33–77.

Gordon, H. R. (1997). Atmospheric correction of ocean color imagery in the Earth Observing System era. *Journal of Geophysical Research-Atmospheres (1984–2012)*, *102*, 17081–17106.

Gower, J., Hu, C., Borstad, G., & King, S. (2006). Ocean color satellites show extensive lines of floating *Sargassum* in the Gulf of Mexico. *IEEE Transactions on Geoscience and Remote Sensing*, *44*, 3619–3625.

Gower, J., & King, S. (2011). Distribution of floating *Sargassum* in the Gulf of Mexico and the Atlantic Ocean mapped using MERIS. *International Journal of Remote Sensing*, *32*, 1917–1929.

Gower, J., King, S., Borstad, G., & Brown, L. (2005). Detection of intense plankton blooms using the 709 nm band of the MERIS imaging spectrometer. *International Journal of Remote Sensing*, *26*, 2005–2012.

Gower, J., Young, E., & King, S. (2013). Satellite images suggest a new *Sargassum* source region in 2011. *Remote Sensing Letters*, *4*, 764–773.

He, M. -X., Liu, J., Yu, F., Li, D., & Hu, C. (2011). *Monitoring green tides in Chinese marginal seas*. Handbook of satellite remote sensing image interpretation: Applications for marine living resources conservation and management. Dartmouth, Canada: EU PRESPO and IOCCG, 111–124.

Hochberg, E. J., Atkinson, M. J., & Andréfouët, S. (2003). Spectral reflectance of coral reef bottom-types worldwide and implications for coral reef remote sensing. *Remote Sensing of Environment*, *85*, 159–173.

Hu, C. (2009). A novel ocean color index to detect floating algae in the global oceans. *Remote Sensing of Environment*, *113*, 2118–2129.

Hu, C., Barnes, B. B., Murch, B., & Carlson, P. (2014). Satellite-based virtual buoy system to monitor coastal water quality. *Optical Engineering*, *53* (051402-051402).

Hu, C., Cannizzaro, J., Carder, K. L., Muller-Karger, F. E., & Hardy, R. (2010). Remote detection of *Trichodesmium* blooms in optically complex coastal waters: Examples with MODIS full-spectral data. *Remote Sensing of Environment*, *114*, 2048–2058.

Hu, C., Feng, L., & Lee, Z. (2013). Uncertainties of SeaWiFS and MODIS remote sensing reflectance: Implications from clear water measurements. *Remote Sensing of Environment*, *133*, 168–182.

Hu, C., Feng, L., Lee, Z., Davis, C. O., Mannino, A., McClain, C. R., et al. (2012). Dynamic range and sensitivity requirements of satellite ocean color sensors: Learning from the past. *Applied Optics*, *51*, 6045–6062.

Hu, C., Lee, Z., & Franz, B. (2012). Chlorophyll-a algorithms for oligotrophic oceans: A novel approach based on three-band reflectance difference. *Journal of Geophysical Research, Oceans*, *117*, C01011 (doi:01010.01029/02011JC007395).

Hu, C., Li, D., Chen, C., Ge, J., Muller-Karger,, F. E., Liu, J., et al. (2010). On the recurrent *Ulva prolifera* blooms in the Yellow Sea and East China Sea. *Journal of Geophysical Research, Oceans*, *115*, C05017 (doi:05010.01029/02009JC005561).

Hu, C., Muller-Karger, F. E., Biggs, D. C., Carder, K. L., Nababan, B., Nadeau, D., et al. (2003). Comparison of ship and satellite bio-optical measurements on the continental margin of the NE Gulf of Mexico. *International Journal of Remote Sensing*, *24*, 2597–2612.

Hu, C., Weisberg, R. H., Liu, Y., Zheng, L., Daly, K. L., English, D. C., et al. (2011). Did the northeastern Gulf of Mexico become greener after the Deepwater Horizon oil spill? *Geophysical Research Letters*, *38*, L09601 (doi:09610.01029/02011GL047184).

Lapointe, B. E. (1995). A comparison of nutrient-limited productivity in *Sargassum natans* from neritic vs. oceanic waters of the western North Atlantic Ocean. *Limnology and Oceanography*, *40*, 625–633.

Lapointe, B. E., West, L. E., Sutton, T. T., & Hu, C. (2014). Ryther revisited: nutrient excretions by fishes enhance productivity of pelagic *Sargassum* in the western North Atlantic Ocean. *Journal of Experimental Marine Biology and Ecology*, *458*, 46–56.

Lee, Z., Carder, K., Arnone, R., & He, M. (2007). Determination of primary spectral bands for remote sensing of aquatic environments. *Sensors*, *7*, 3428–3441.

Lee, Z., Shang, S., Hu, C., & Zibordi, G. (2014). Spectral interdependence of remote-sensing reflectance and its implications on the design of ocean color satellite sensors. *Applied Optics*, *53*, 3301–3310.

Lucke, R. L., Corson, M., McGlothlin, N. R., Butcher, S. D., Wood, D. L., Korwan, D. R., et al. (2011). Hyperspectral Imager for the Coastal Ocean: Instrument description and first images. *Applied Optics*, *50*, 1501–1516.

Marmorino, G. O., Miller, W., Smith, G. B., & Bowles, J. H. (2011). Airborne imagery of a disintegrating *Sargassum* drift line. *Deep Sea Research Part I: Oceanographic Research Papers*, *58*, 316–321.

Mehrtens, C., Kaschell, T., Tardeck, F., Graser, N., Borowy, C., & Bartsch, I. (2009). Differentiation of brown seaweeds by hyperspectral airborne remote sensing and field spectrometry in a rocky intertidal. *Sixth EARSel SIG IS workshop* (pp. 16–19) (March 2009).

Moore, T. S., Campbell, J. W., & Feng, H. (2014). Characterizing the uncertainties in spectral remote sensing reflectance for SeaWiFS and MODIS-Aqua based on global in situ matchup data sets. *Remote Sensing of Environment*, *159*, 14–24.

Mueller, J. L., Bidigare, R., Trees, C., Balch, W., Dore, J., Drapeau, D., et al. (2003). *Ocean optics protocols for satellite ocean color sensor validation, revision 5, volume V: Biogeochemical and bio-optical measurements and data analysis protocols*. NASA Tech. Memo, 211621, 36.

Pahlevan, N., Lee, Z., Wei, J., Schaaf, C. B., Schott, J. R., & Berk, A. (2014). On-orbit radiometric characterization of OLI (Landsat-8) for applications in aquatic remote sensing. *Remote Sensing of Environment*, *154*, 272–284.

Powers, S. P., Hernandez, F. J., Condon, R. H., Drymon, J. M., & Free, C. M. (2013). Novel pathways for injury from offshore oil spills: Direct, sublethal and indirect effects of the Deepwater Horizon oil spill on pelagic *Sargassum* communities. *PloS One*, *8*, e74802.

Qi, L., Hu, C., Duan, H., Cannizzaro, J., & Ma, R. (2014). A novel MERIS algorithm to derive cyanobacterial phycocyanin pigment concentrations in a eutrophic lake: Theoretical basis and practical considerations. *Remote Sensing of Environment*, *154*, 298–317.

Rooker, J. R., Turner, J. P., & Holt, S. A. (2006). Trophic ecology of *Sargassum*-associated fishes in the Gulf of Mexico determined from stable isotopes and fatty acids. *Marine Ecology Progress Series*, *313*, 249–259.

Son, Y. B., Min, J. -E., & Ryu, J. -H. (2012). Detecting massive green algae (*Ulva prolifera*) blooms in the Yellow Sea and East China Sea using geostationary ocean color imager (GOCI) data. *Ocean Science Journal*, *47*, 359–375.

Suwandana, E., Kawamura, K., Sakuno, Y., Evri, M., & Lesmana, A. H. (2012). Hyperspectral reflectance response of seagrass (*Enhalus acoroides*) and brown algae (*Sargassum* sp.) to nutrient enrichment at laboratory scale. *Journal of Coastal Research*, *28*, 956–963.

Szekielda, K. H., Marmorino, G. O., Bowles, J. H., & Gillis, D. (2010). High spatial resolution spectrometry of rafting macroalgae (*Sargassum*). *Journal of Applied Remote Sensing*, *4* (043529–043529-043513).

Tsoar, H. (2005). Sand dunes mobility and stability in relation to climate. *Physica A: Statistical Mechanics and its Applications*, *357*, 50–56s.

Witherington, B., Hirama, S., & Hardy, R. (2012). Young sea turtles of the pelagic *Sargassum*-dominated drift community: Habitat use, population density, and threats. *Marine Ecology Progress Series*, *463*, 1–22.

Zepp, R., Shank, G., Vähätalo, A., Bartels, E., & Jones, R. (2008). Photobiogeochemistry of *Sargassum*: A potentially important source of chromophoric dissolved organic matter in the upper ocean. *Ocean Science Meeting, 2–7 March 2008* (Orlando, Florida, U.S.A.).